ResearchGate

See discussions, stats, and author profiles for this publication at: https://www.researchgate.net/publication/321814979

Defining the natural fracture network in a shale gas play and its cover succession: The case of the Utica Shale in eastern Canada

Article *in* Journal of Structural Geology · December 2017

DOI: 10.1016/j.jsg.2017.12.007

CITATIONS
20

READS
665

6 authors, including:

Pierre Ladevèze
Institut National de la Recherche Scientifique
12 PUBLICATIONS **136** CITATIONS

SEE PROFILE

Christine Rivard
Natural Resources Canada
86 PUBLICATIONS **1,189** CITATIONS

SEE PROFILE

Denis Lavoie
Natural Resources Canada
309 PUBLICATIONS **4,224** CITATIONS

SEE PROFILE

All content following this page was uploaded by René Lefebvre on 19 December 2017.

The user has requested enhancement of the downloaded file.

Defining the natural fracture network in a shale gas play and its cover succession: the case of the Utica Shale in eastern Canada

Ladevèze, P. [*,a,b], Séjourné, S.[c], Rivard, C. [b], Lavoie, D. [b], Lefebvre, R.[a], Rouleau, A.[d]

[a] *INRS – Centre Eau Terre Environnement, 490 rue de la Couronne, Québec City, QC G1K 9A9, Canada*

[b] *Geological Survey of Canada – Québec, 490 rue de la Couronne, Québec City, QC G1K 9A9, Canada*

[c] *Enki GéoSolutions, Montréal, Canada*

[d] *UQAC, 555 Blvd. de l'Université, Chicoutimi, QC G7H 2B1, Canada*

[*] *Corresponding author: pierrelad@gmail.com*

Keywords: natural fracture characterization; analogs; conceptual models; shale gas; Utica Shale

Abstract

In the St. Lawrence sedimentary platform (eastern Canada), very little data are available between shallow fresh water aquifers and deep geological hydrocarbon reservoir units (here referred to as the intermediate zone). Characterization of this intermediate zone is crucial, as the latter controls aquifer vulnerability to operations carried out at depth. In this paper, the natural fracture networks in shallow aquifers and in the Utica shale gas reservoir are documented in an attempt to indirectly characterize the intermediate zone. This study used structural data from outcrops, shallow observation well logs and deep shale gas well logs to propose a conceptual model of the natural fracture network. Shallow and deep fractures were categorized into three sets of steeply-dipping fractures and into a set of bedding-parallel fractures. Some lithological and structural controls on fracture distribution were identified. The regional geologic history and similarities between the shallow and deep fracture datasets allowed the extrapolation of the fracture network characterization to the intermediate zone. This study thus highlights the benefits of using both datasets simultaneously, while they are generally interpreted separately. Recommendations are also proposed for future environmental assessment studies in which the existence of preferential flow pathways and potential upward fluid migration toward shallow aquifers need to be identified.

1 Introduction

For shale-dominated successions, there is a high interest in identifying natural fracture networks because they control the rock permeability (Barton et al., 1998; Berkowitz, 2002; Guerriero et al., 2013; Narr et al., 2006; Odling et al., 1999; Singhal and Gupta, 2010) and thus strongly influence fluid flow in the different stratigraphic units and potentially between deep prospective shale gas strata and shallow aquifers (CCA 2014; EPA 2016; Lefebvre, 2016).

However, the quantitative assessment of natural fractures can be challenging due to observational biases related to the methods that provide results at different scales (e.g. at the scale of outcrops, wells or seismic lines) and to the data that are sparsely or irregularly distributed. The inherent incompleteness of data is exacerbated in the so-called "intermediate" zone (or caprock). There is generally a lack of observation in this zone because it is located between shallow aquifers studied for hydrogeological purpose and the deep reservoir that has been characterized for hydrocarbon exploration/production. The characterization of this zone is crucial to properly understand the dynamic of potential contaminants migration to shallow aquifers.

Fracture observations on outcrops are often used as analogs for deep reservoirs (Antonellini and Mollema, 2000; Gale et al., 2014; Larsen et al., 2010; Lavenu et al., 2013; Vitale et al., 2012). Hence, the extrapolation of fracture data from outcrops and shallow hydrogeological wells, or from the deep reservoir where well log data and other geoscience information abound, may appear to be a promising approach to characterize the intermediate zone. However, the use of 'shallow' or 'deep' datasets as analogs is not always possible and certainly not straightforward; the controls on fracture distribution in a sedimentary succession have to be carefully identified to fully assess the fracture patterns. At shallow depths, surface weathering can enhance fracture apertures and be possibly responsible for fractures filling with minerals that are not representa-

tive of deep units. Furthermore, uplift or unroofing can initiate fracture propagation (Engelder, 1985; English, 2012; Gale et al., 2014). Therefore, the presence of unloading fractures oriented according to either a residual or a contemporary stress field will affect the shallow rock mass (Engelder, 1985). To the contrary, some fracture generation processes can occur only at significant depths due to an increase of the greatest compressive stress during regional shortening, a decrease in the least compressive stress caused by regional extension or an increase in pore pressure (Gillespie et al., 2001). Therefore, to be able to use some shallow and deep fracture sets as analogs, it must first be demonstrated that outcropping fractures are not solely the expression of near-surface events and were most likely formed at significant depths (at least comparable with the reservoir depth).

In this paper, we aim at integrating multisource data (outcrops, shallow and deep acoustic and electric well logs) that have different observation scales to obtain a sound interpretation of the fracture network affecting a shale gas play in southern Quebec (Saint-Édouard area, approximately 65 km southwest of Quebec City; location in Fig. 1). An emphasis is put on the characterization of the intermediate zone which potentially controls contaminants migration to subsurface. The proposed methodology could be of interest for other studies in shale dominated successions where there is a lack of data in the intermediate zone.

2 Regional tectonostratigraphic setting

2.1 *The St. Lawrence Platform*

In southern Quebec, the St. Lawrence Platform is bounded by the Canadian Shield to the NW and by the Appalachian mountain belt to the SE. The portion of interest of the St. Lawrence Platform (here referred as the SLP) comprises the area roughly between Montréal and Quebec City. This Cambrian-Ordovician depositional element is divided in two tectonostratigraphic domains: the autochthonous and the parautochthonous domains (Castonguay et al., 2010; St-Julien and Hubert, 1975) (Fig. 1). At the base of the autochthonous domain, Cambrian-Ordovician rift and passive margin units unconformably overlie the Grenville crystalline rocks (Lavoie et al., 2012) (Fig. 2). These passive margin units include the Potsdam Group sandstones and conglomerates and the Beekmantown Group dolomites and limestones. Those two groups are covered by Middle to Upper Ordovician units deposited in a foreland basin setting (Lavoie, 2008) (Fig. 2). The progressively deepening-upward carbonate units of the succeeding Chazy, Black River and Trenton groups, and the Utica Shale, were then covered by the overlying Upper Ordovician turbidite and molasse units of the Sainte-Rosalie, Lorraine and Queenston groups. The Utica Shale constitutes a prospective unit for shale gas in southern Quebec (Dietrich et al., 2011; Hamblin, 2006; Lavoie, 2008; Lavoie et al., 2014).

The SLP units have recorded a polyphased structural history (Pinet et al., 2014) and thus display a complex structural pattern. These events include Middle and Late Ordovician normal faulting that started at the inception of the foreland basin phase (Thériault, 2007), shortening during the Taconian orogeny (Tremblay and Pinet, 2016), and some post-Ordovician folding (Pinet et al., 2008) and faulting (Sasseville et al., 2008; Tremblay et al., 2013). Normal faults (including the Jacques-Cartier River fault, Fig. 5) are steeply-dipping to the south and displace the basement,

97 the basal units of the platform and its upper units in the autochthonous domain (possibly includ-
98 ing the Utica Shale and Lorraine Group). These faults were reactivated several times during and
99 after the building of the Appalachians, documented evidence of movement is known for the late
100 Silurian Salinic Orogeny and the opening of modern Atlantic (Castonguay et al., 2001; Faure et
101 al., 2004; Konstantinovskaya et al., 2009; Sasseville et al., 2012; Séjourné et al., 2003; Tremblay
102 and Pinet, 2016). A summary of the depositional environment and the major tectonic events that
103 affected rock of the SLP is presented in Fig. 3.

104 In the autochthonous domain, the near surface Upper Ordovician units (post-Utica Shale) are
105 folded by the regional Chambly-Fortierville syncline. This fold is asymmetric with more steeply-
106 dipping beds in the southern flank (28°) than in the northern flank (10°) (Fig. 4a). Its axis is
107 roughly parallel to the limit between the SLP and the Appalachians. To the southeast, the Aston
108 fault and the Logan's Line belong to a regional thrust-fault system that limits the parautochtho-
109 nous domain (Fig. 2 and Fig. 5). Reprocessing and reinterpretation of an industrial 2D seismic
110 line (using two well calibration points) was proposed in (Lavoie et al., 2016) and showed that in
111 the Saint-Édouard area, the parautochthonous domain forms a triangle zone delimited to the
112 northwest by a NW-dipping backthrust and by the SW-dipping the Logan's Line to the SE (Fig.
113 5). The existence of a triangle zone bounding the southern limb of the Chambly-Fortierville is
114 supported by previous interpretations done in the SLP (Castonguay et al., 2006; Castonguay et
115 al., 2003; Konstantinovskaya et al., 2009). These thrusts/backthrusts are associated with the
116 Middle to Late Ordovician Taconian Orogeny (St-Julien and Hubert, 1975). In the parautochtho-
117 nous domain, a southeast-dipping system of thrust faults displays imbricated thrust geometries
118 (Castonguay et al., 2006; Séjourné et al., 2003; St-Julien et al., 1983). Some northeast-striking
119 folds also affect the parautochthonous units (Fig. 4b). The Logan's Line marks the fault-contact

between the SLP and the allochthonous external Humber zone (St-Julien and Hubert, 1975) (Fig. 5).

The present-day in-situ maximum horizontal stress (SH_{max}) orientation is NE–SW in the SLP as previously proposed using borehole breakouts orientations (inferred from four-arm dipmeter caliper data) (Konstantinovskaya et al., 2012). This trend is relatively consistent with the large-scale trend documented in eastern North America (Heidbach et al., 2009; Zoback, 1992). The stresses/pressure gradients estimated in the platform indicate a strike-slip stress regime (Konstantinovskaya et al., 2012). As the regional faults of the SLP are oblique to the actual SH_{max}, a reactivation of these structures under the current stress field remains possible (Konstantinovskaya et al., 2012) but has not yet been documented.

Organic matter reflectance data indicates that at least 3 and 4.7 km of sediments have been eroded in the SLP (Sikander and Pittion, 1978) and in the frontal part of the Chaudière Nappe in the Quebec City area (Ogunyomi et al., 1980), respectively. Later studies showed that there was an increasing thickness of eroded sediments from about 5 to 7 km from northeast to southwest in the SLP (Héroux and Bertrand, 1991; Yang and Hesse, 1993).

2.2 *The intermediate zone (caprock) and reservoir units of the Saint-Édouard area*

The Utica Shale is overlain by autochthonous units (the Nicolet Formation - Lorraine Group and the Lotbinière Formation – Sainte-Rosalie Group) and parautochthonous units (Les Fonds Formation – Sainte-Rosalie Group). These units constitute the intermediate zone (caprock) in the Saint-Édouard study area.

The Utica Shale (Upper Ordovician) is made of limy mudstone that contains centi- to decimetric interbeds of shaley limestone (Globensky, 1987; Lavoie et al., 2008; Theriault, 2012). It is divid-

142 ed in two members (Upper and Lower). The Lower Utica Shale contains more limestone inter-
143 beds than the Upper Utica Shale. In the Saint-Édouard area, the thickness of the Utica Shale
144 ranges from 200 to 400 m (Fig. 5). The autochthonous Lotbinière Formation (Sainte-Rosalie
145 Group) and the parautochthonous Les Fonds Formation (Sainte-Rosalie Group) are time- and
146 facies correlative units of the Utica Shale (Lavoie et al., 2016) (Fig. 2). The Utica Shale, Lotbi-
147 nière and Les Fonds formations display a similar lithofacies of black calcareous mudstone with
148 thin beds of impure fine-grained limestone but differs by their organofacies (Lavoie et al., 2016).
149 The Lotbinière Formation is made of gray-black micaceous shale with rare interbeds of calcare-
150 ous siltstones (thickness <10 cm) and is outcropping north of the Jacques-Cartier River normal
151 fault (Belt et al., 1979; Clark and Globensky, 1973). In the parautochthonous domain, the Les
152 Fonds Formation is mainly composed of shale with less abundant fine-grained limestones and
153 conglomerates (Comeau et al., 2004). The Nicolet Formation (Lorraine Group, Upper Ordovi-
154 cian) is slightly younger compared to the previous three units (Comeau et al., 2004) and is most-
155 ly made of gray to dark-gray shale with centi- to decimetric (rarely metric) siltstone interbeds
156 (Clark and Globensky, 1973; Globensky, 1987). Upward, there is a decrease of the shale content
157 and an increase in the number and thickness of the sandstone beds (Clark and Globensky, 1976).
158 In the Saint-Édouard area, the thickness of autochthonous and parautochthonous intermediate
159 zone units (i.e., above the Utica Shale) progressively increases from 400 m to 1900 m from
160 northwest to southeast (Fig. 5).

161

162 **Insert Fig. 1 to 5 here.**

163

164 **3 Methodology**

In this study, the term “fracture” refers to metric scale planar discontinuities that affect the rock mass without visible displacement.

3.1 *Data sources*

Fracture data were collected and compiled in the Saint-Édouard area using different methods. Fifteen outcrops were investigated (Fig. 1). Borehole logs includes acoustic, optical and electric logs that have different resolutions. Typically, electric logs have a higher resolution than acoustic and optical tools. Interpretation were then done in the light of these scale differences. Acoustic and optical televiewer logs from eleven shallow (15 to 147 m deep in the bedrock) groundwater monitoring wells drilled for the project (Crow and Ladevèze, 2015) were also studied. Moreover, Formation Micro Imager (FMI) data from three deep shale gas wells were interpreted. The wells referenced by the oil and gas geoscience information system of the Ministère des Ressources naturelles of Quebec under the numbers A266/A276 (Leclercville n°1), A279 (Fortierville n°1) and A283 (Sainte-Gertrude n°1) were used. To simplify the nomenclature in the current paper, they are hereafter referred to as A, B and C, respectively (Fig. 1). FMI data from the vertical sections of wells A, B and C cover the following ranges of depth: 1470-2080 m for well A, 560-2320 m for well B and 590-2050 m for well C; this includes the Utica Shale and variable portions of the overlying Lorraine Group. Each of these wells also includes a horizontal section (“horizontal leg”) in the Utica Shale (1000, 970 and 920 m long, for wells A, B and C respectively) for which FMI data was also available. For a history of the recent shale gas exploration in the study area, refer to Lavoie et al. (2014) and Rivard et al. (2014). The characteristics of the measurement stations are summarized in Table 1.

Insert Table 1 here.

188

189 3.2 *Fracture assessment*

190 Common geometrical attributes of fractures were measured: attitude, spacing, crosscutting rela-
191 tionships between fractures and other geological structures (such as syn-sedimentary concre-
192 tions). These attributes were documented all along the boreholes using acoustic and electrical
193 logs. As most of the outcrops were limited in size and were displaying only sparsely distributed
194 fractures, their attributes were systematically measured in the exposed surfaces.

195 *3.2.1 Fracture sets*

196 For each measurement station (outcrop or well), fracture poles were plotted on stereonets using
197 the *SpheriStat*™ software (Stesky, 2010). Contoured density diagrams were used to identify the
198 mean position of the fracture sets. The poles density contours of borehole data were corrected for
199 sampling bias (underestimation of the frequencies for the fracture planes that are sub-parallel to
200 the observation line) using the method of Terzaghi (1965). A weight function of the angle β be-
201 tween the fracture plane and the observation line was attributed to all fracture densities. This
202 weight w is expressed as: $w=(\sin \beta)^{-1}$ (Terzaghi, 1965). Even if mathematically valid, fracture
203 planes with low β values are overestimated with this method (Park and West, 2002). For this
204 reason, an arbitrary 10° blind zone was used in the analysis (fractures sub-parallel to the observa-
205 tion-line are excluded).

206 When clear crosscutting relationships were observed on outcrops, the relative timing of fracture
207 sets formation could be defined. In borehole data, it was rarely possible to identify such relation-
208 ships. In this case, the main attitude for fracture set attitudes were compared to adjacent outcrops
209 data (if existing) to define a hypothetical relative timing for the formation of the fracture sets.

If fracture poles are scattered in stereonets, only the maximum pole concentration is taken into account. To better identify the major fracture sets in such cases (generally the case of outcrops or shallow wells that displays significant folding), a fold test was performed on fracture data in order to calculate the fracture attitudes prior to folding events. Results from this test were also used to further assess the relative chronology of fracture sets formation and folding. The rotation applied to fracture attitudes corresponds to the angle of rotation of the bedding plane after a folding event. Two generations of folds have previously been documented in the autochthonous domain in the Saint-Édouard area: F-I (first generation: Chambly-Fortierville syncline) and F-II (second generation) (Pinet, 2011). To consider the effect of the two generations of folds, the analysis was performed in two steps. First, the fracture plans were replaced back to their original attitude prior to F-II folding. As the F-II fold axes are sub-horizontal, the first step consists in correcting the strike direction of fracture planes according to the strike angle between fold-I and fold-II axes. The second step aims at correcting the fracture plans back to their attitude prior to F-I folding. This was done by tilting back the fracture planes around the F-I axis (N233/04, Fig. 4) with an angle corresponding to the structural dip (angle between the bedding plane attitudes in each measurement station and the horizontal). In the parautochthonous domain, a single folding event was easily observable in the field and fracture plans were back-tilted along the regional F-I axis (N235/03 Fig. 4). A better fracture set concentration after rotation is a strong indicator of its pre-folding origin. To quantify the degree of concentration of attitude data, the parameter k was calculated for both the original and rotated fracture sets. This parameter quantifies the degree of data dispersion on a sphere/stereonet (Fisher, 1953). The higher the values of k, the more the data are concentrated in the stereonet (Fiore Allwardt et al., 2007).

3.2.2 Fractures distribution

In the document, the term “spacing” refers here to the perpendicular distance between two adjacent fracture planes of similar attitude. Measuring or estimating spacing thus requires first a classification of the fractures into coherent fracture attitude set. The fractures densities correspond to the number of fractures (regardless of their attitudes) per unit distance along a line. They were calculated along the wells using a counting window of various lengths. Each fracture density value was then normalized by the window lengths. All fracture densities were corrected using the Terzaghi method. In the same way, fracture frequencies correspond to the number of fractures from a specific set per unit distance along a line.

To further explore the process of fracturing in siltstone units, the fracture spacing was plotted against bed thicknesses (fractures are bed-confined in siltstone to the contrary of shale in the studied area). Values of the ratio of fracture spacing to layer thickness (the slope of the curve) were extracted from these plots and used to determine if the fracture network has attained saturation, a concept describing the situation where whatever the applied strain, fracture spacing has attained a lower limit (or an upper limit for fracture densities) that is proportional to bed thickness (Bai et al., 2000; Wu and D. Pollard, 1995).

Geostatistical tools were used to assess the degree of spatial correlation of each fracture set (Chilès, 1988; Escuder Viruete et al., 2001; Miller, 1979; Tavchandjian et al., 1997; Valley, 2007; Villaescusa and Brown, 1990). In other words, the use of geostatistics can help define the spatial organization of fractures when they seem to have a totally random spatial distribution in the rock mass. The knowledge of the spatial distribution of fractures can be used to develop discrete fracture network (DFN) models to further assess the fracture control on fluid flow (Caine and Tomusiak, 2003; Dershowitz et al., 1998; Min et al., 2004; Surrette et al., 2008).

Variogram analyses were thus performed on spacing data for each fracture set in the horizontal section of the three deep wells. A formal definition of the experimental variogram γ(h) (m^2) for fracture spacing data is presented in Eq. (1).

$$\gamma(h) = \frac{1}{2n}\sum_{i=1}^{n}\left[z(x_i) - z(x_i + h_i)\right]^2 \qquad \text{Eq. (1)}$$

where, n is the number of fractures separated by a distance h (this calculation interval is also called "lag"), $z(x_i)$ is the fracture spacing value at the distance x_i. An experimental variogram presents the γ values successively calculated for increasing h values. The shape of the experimental variogram is used to assess if the available data have a spatial correlation that could be represented by a theoretical model. If so, the nugget value in the experimental variogram must be lower than the variance of the entire dataset for the correlation in fracture spacing to be considered present (reflecting fracture clustering). The range value in the variogram provides the maximum distance for fracture spacing clustering. In geological terms, this range of influence means that two samples spaced farther apart than this distance are likely not correlated (and thus considered independent) (Miller, 1979).

3.2.3 Fracture and rock mechanical properties

The potential for fracture propagation in rocks is controlled by their brittleness (Ding et al., 2012; Lai et al., 2015; Meng et al., 2015). The Brittleness Index is an empirical parameter that is widely used to quantify the ability of a rock unit to fracture (Wang et al., 2015). In the Saint-Édouard area, this parameter was previously estimated from borehole logs acquired in the deep gas wells using the Grieser and Bray (2007) and the Glorioso and Rattia (2012) methods (Séjourné, 2017). These methods are respectively based on the acoustic (compressional and shear wave velocity logs) and mineralogical (derived from elemental spectroscopy logs) properties of

277 the shale. In the current paper, the relationship between fracture densities and brittleness varia-
278 tions in the Lorraine Group and Utica Shale was explored.

279 **4 Results**

280 4.1 *Fractures in shales*

281 Two fracture types were observed in shale units: steeply-dipping fractures (F1, F2 and F3) and
282 bedding-parallel fractures (BPF). Examples of observed fractures on outcrops are presented in
283 Fig. 6. In the vast majority of outcrops, fractures are planar and exhibit clear crosscutting rela-
284 tionships. For this reason, it was possible to sort the high-angle fractures in three sets that are
285 designated according to their relative order of formation (F1, F2 and F3 sets; F1 is the older set).
286 Fractures were also only bed-confined in siltstones.

287 To facilitate the classification of fractures in sets, a fold test analysis was done using data from
288 outcrops and shallow wells that were affected by folding events that could be clearly identified in
289 the field (i.e. outcrops affected by folds F-II and F-I). Fracture attitudes from outcrops and values
290 of the associated parameter *k* (which quantifies the data concentration in the stereonets) are pre-
291 sented in Fig. 8. In the autochthonous domain, an improved concentration of fracture poles was
292 obtained for F1 and F2 sets after rotation prior to the second generation of folds (F-II). Then,
293 removing the effects of F-I fold improved even more the concentration of F1 fractures, but had
294 no effect on the concentration of F2 fractures. This strongly suggests a pre-F-I folding origin for
295 the F1 set, and a pre- to syn-F-II origin for F2 fractures. To the contrary, the concentration of the
296 F3 fracture set was reduced after removing both F-II and F-I effects, thus supporting a syn- to
297 post F-II folding origin for this F3 set. One fold generation was clearly observed in the parau-
298 tochthonous domain (other fold generations may exist but were hardly observable on outcrops).

299 This regional folding corresponds to the first fold generation (F-I) documented in the autochtho-
300 nous domain. The fold test showed that a better concentration was obtained for the F1 set when
301 rotated prior to folding, confirming a potential pre-F-I origin for F1 fractures. Results for the F2
302 fracture set show a slight, probably poorly significant, reduction of concentration and the timing
303 remains not well constrained on the basis of the fold test.

304 Fracture sets F1 and F2 are pervasive in both the autochthonous and parautochthonous domains.
305 They strike NE (F1) and NW (F2) (Fig. 7), with F2 abutting against F1 (Fig. 6a and b). F1 and
306 F2 are perpendicular to each other and orthogonally crosscut the bedding planes (S0). F1 frac-
307 tures are locally concentrated in corridors (as in Fig. 6b). The third fracture set (F3) is only doc-
308 umented in the autochthonous domain. F3 strikes WNW and is sub-vertical (dip >80°) whatever
309 the bedding planes attitudes (Fig. 7). F3 generally crosscuts F1 and F2 and was not observed at
310 all sites. All three fracture sets were documented in shallow and deep data. Finally the BPF were
311 only observed at shallow depth.

312 Detailed fracture length measurements were limited to the size of the outcrops. Thus, only semi-
313 quantitative fracture length estimations are here proposed. Fracture lengths for the F1 and F2 sets
314 were approximately between 2 and 5 m. The maximum observed fracture lengths were ranging
315 between 10 and 30 m. F1 fractures display lengths higher than F2 fractures, as F2 abut F1 frac-
316 tures. Due to the limited number of outcropping F3 fractures, no realistic estimate of fracture
317 lengths for this set was possible. Finally, because some fractures locally extend beyond the limit
318 of the outcropping areas, length estimation values must be considered with caution.

319 Some intervals in the black shales of the Lotbinière Formation (northern part of the study area)
320 display oval-shaped carbonate concretions (maximum diameter of up to 1.5 m; length-to-width
321 ratio around 1.5). The metabolic activity of sulfate-reducing and methanogen bacteria that oc-

curred shortly after the inception of burial of organic matter-rich sediments under anoxic conditions are responsible for the formation of these concretions (Mozley and Davis, 2005). In the Lotbinière Formation, 15 fractures were identified passing around such concretions without crosscutting them (Fig. 6c). Such a relationship is interpreted as an indicator of natural fractures propagation in the presence of abnormal fluid pressure in response to the shale thermal maturation and to the gas generation in a context of deep burial (McConaughy and Engelder, 1999).

Insert fig. 6 to 8 here.

Statistics on fracture spacing data from outcrops and boreholes are presented in Fig. 9. Median values in shale outcrops are significantly for F1 than for F2 (0.20 to 0.28 m for F1; 2.4 to 2.93 m for F2). The same trend is observed in the shale gas wells (0.14 m for F1 and 2.93 m for F2). Lower and upper quartiles for fracture spacing also extend over a significantly larger interval for the F2 set than for the F1 set, suggesting a more scattered spatial distribution of F2 fractures, especially in the Utica Shale. In the deep wells, the mean value for F3 spacing (0.11 m) is slightly lower than that of the F1 value.

Insert fig. 9 here.

To the contrary of F2 fractures, both F1 and F3 fractures spacing data from outcrops and shale gas wells seems to follow a power law distribution (exponent values around 1), see Fig. 10. In this figure, spacing value less than 0.05m (resolution of the observation methods) and higher

than 10 m (upper limit of statistical homogeneity) were excluded for the regression calculation. Following Bonnet et al. (2001), this may reflect the scale invariance of the fracture spacing for these two sets. The existence of the power law distribution must be interpreted with care as our dataset is affected by both censoring bias (high fracture spacing is not sampled due to the limited size of outcrops and well sections) and truncation bias (limitation due to tools resolution). Then, the scale range of observations did not extend two orders of magnitude as suggested by Bonnet et al. (2001). Despite this limitation, the specific trend for F2 fractures distribution may be explained by the relative timing of fracture formation. If F2 fractures lengths are constrained by F1 spacing, F2 spacing may not be scale invariant. This further support the possibility of a successive formation of F1 and F2 fractures.

Insert fig. 10 here.

All experimental variograms of the fracture sets obtained from horizontal legs of wells A, B and C show nugget values much lower than the variance of the entire sample (Fig. 11), implying that there is a correlation in fracture spacing. Therefore, fracture distributions display some clustering. F1 fractures display ranges values between 30 and 150 m. Variograms for the F2 and F3 set display ranges from 12 to 30 m, and 60 to 100 m respectively. Some concentration of F1 fractures (with significantly higher F1 fracture frequencies than other fracture sets) were identified in the horizontal well A (in the Utica Shale). This high frequency of F1 fractures is consistent with outcrop observations where F1 fractures spacing are lower than F2 and F3 spacing. This may be interpreted as the presence of F1 fractures corridors (see for instance Fig. 12: F1 fractures are closely spaced on distances of around 40 m and separated by approximately 100 to 200 m).

Insert fig. 11 and 12 here.

In the deep zone, fracture density vertical profiles generally display localized fractured intervals separated by vertical distances ranging from 10 m to 300 m. Fig. 13 only presents the fracture density and Brittleness Index (BI) variation with depth for well B, but they can be considered representative of those found in wells A and C. Higher fracture densities and BI values were generally measured in the Utica Shale. This suggests that these two parameters could be correlated. In specific depth intervals in well B, some high fracture densities values correlates with low BI values (see the contact between the Upper and Lower Utica in Fig. 13). Geomechanical contrasts in the vicinity of these lithological contacts may explain the occurrence of these higher fracture density intervals.

Insert fig. 13 here.

4.2 *Fractures in siltstone interbeds*

Data from outcrops showed that the siltstone interbeds are crosscut by the same fracture sets as those cutting across the shale (F1, F2 and F3) (Fig. 14a and b). However, contrary to shale units, fractures are stratabound in siltstone units, with only a few F1 fractures intersecting both siltstone and shale beds (Fig. 14c). F1 fractures are also generally longer than F2 fractures. F2 fractures abut F1 fractures and F2 fracture lengths generally equal to F1 fracture spacings (Fig. 14b). Fracture density in the siltstone beds is significantly higher than in shale intervals, with spacings

lower than 1 m for both F1 and F2 fracture sets. Fractures were regularly spaced all along the outcrops. There is also a strong correlation between siltstone bed thickness and fracture spacing as shown in Fig. 15b. The calculated ratios of fracture spacing to layer thickness are respectively 1.29 and 1.43 for the F1 and F2 fracture sets.

Insert fig. 14 and 15 here.

5 Discussion

5.1 *Fracture pattern*

5.1.1 Main controls on fracture distributions

The differences in fracture distribution between the Lorraine Group shales and the Lorraine Group siltstones, and also between the Lorraine Group shales and the Utica Shale, suggest that these distributions are lithologically controlled.

Differences in fracture distributions were observed between shales and siltstones of the Lorraine Group. In Lorraine Group shales, the F1 spacing is lower than the F2 spacing (see a visual example in Fig. 6b) and F1 and F2 fracture are probably organized in corridors. In siltstone units of the Lorraine Group, F1 and F2 fractures are more homogeneously distributed and display equivalent spacing values (see a visual example in Fig. 14). Fractures in siltstone units are also limited by the bed thickness (which rarely exceeds 1 to 2 m) and this parameter is correlated with fracture spacing (Fig. 15); this was also observed in many sedimentary basins (Bai et al., 2000; Gross, 1993; Ji and Saruwatari, 1998; Ladeira and Price, 1981; Narr and Suppe, 1991). It was

thus possible to evaluate the fracture saturation in siltstones, based on estimated fracture spacing to layer thickness ratios. According to the threshold interval of ratio values (0.8 to 1.2) proposed in Bai and Pollard (2000) and Bai et al. (2000), F1 and F2 fracture spacing would be at saturation in siltstone units (ratios of 1.29 and 1.43 respectively above the threshold interval of ratio values). Contrasts in mechanical properties between shales and sandstones (the sandstone being more brittle with a higher Young's modulus) induce a preferential fracturing of sandstones (Engelder, 1985; Laubach et al., 2009). This could explain the higher observed fractures densities in the siltstones of the SLP. However, this must be considered cautiously as mechanical property differences between siltstone and shale units were not estimated throughout the SLP. This estimation is challenged by the presence of a significant amount of clay in both units (Séjourné et al., 2013); see also the low BI variations in the proximity of siltstone/shale contacts (Fig. 13).

In the vertical sections of deep shale gas wells (depths > 500 m), higher fracture densities were measured in the Utica Shale compared to the Lorraine Group shales (Fig. 13). This is in agreement with the highly fractured horizontal portions of the shale gas wells completed into the Utica Shale compared to the lower density of steeply-dipping fractures observed in the outcropping Lorraine Group units. In contrast, fracture spacing and strike direction values are similar in the outcropping Lorraine Group units and in the deep Utica Shale (Fig. 7 and Fig. 9). This could be interpreted as fracture corridors being more common in the Utica Shale compared to caprock units. Therefore, when drilling a well through the entire sedimentary succession, there is higher probability of intersecting fracture swarms in the Utica Shale than in overlying units. The Utica Shale is more calcareous than the clayey Lorraine Group shale (Globensky, 1987; Lavoie et al., 2008; Theriault, 2012) resulting in overall higher Brittleness Index (BI) values for the Utica

433 Shale than the overlying shale units (Séjourné, 2017). Brittle shale units are more likely to be
434 affected by a dense natural fracture network than ductile shale (Ding et al., 2012; Lai et al.,
435 2015).

436 *5.1.2 Use of analogs to characterize the caprock*

437 The relationships between the three fracture sets (F1, F2 and F3) and the two regional fold gen-
438 erations was assessed by applying a fold test on shallow fractures. This analysis supports a syn-
439 to post F-II folding origin for the F3 set. Conversely, the F1 and F2 fractures were probably de-
440 veloped before (or possibly during for F2) the main deformation/folding episodes that shaped-up
441 the SLP (F-II and F-I folds). Therefore, the nowadays shallow structures should have been
442 formed at depth before the removal of the overburden by erosion. The presence at reservoir
443 depths of F3 fractures also discards their potential shallow formation after erosion.

444 Vitrinite reflectance data has shown that, at least regionally, around 5 km of overburden have
445 been eroded in the SLP (Héroux and Bertrand, 1991; Yang and Hesse, 1993). At these depths,
446 the fractures propagate according to the regional stress field orientation and thus display com-
447 mon orientations. Because shallow and deep fracture networks display common characteristics
448 (especially in terms of fracture attitudes and spacing) and because of the burial history of the
449 Saint-Édouard area, it is suggested that shallow fractures in shallow units were formed at depth
450 and hence, had recorded the same tectonic events as fractures in deep units. Consequently, shal-
451 low and deep observations can be used to assess the fracture pattern in the intermediate zone.

452 No conclusion can be drawn regarding the initiating mechanism for fracture propagation. The
453 latter could result from an increase of the greatest compressive stress during regional shortening,
454 a decrease in the least compressive stress caused by regional extension, or an increase in pore
455 pressure (which could also be associated with the first two mechanisms). It must be noted that an

456 abnormal pore pressure related to the thermal maturation of organic matter is more likely to have
457 occurred in the Lotbinière Formation, Les Fonds Formation and Utica Shale, as these units dis-
458 play higher organic content than the Lorraine Group units (Haeri-Ardakani et al., 2015; Lavoie et
459 al., 2016). In the Lotbinière Formation, the crosscutting relationship between fractures and cal-
460 careous concretions indicated that some fractures could have been initiated in a context of ab-
461 normal pore pressure.

462 The use of analogs can be controversial if the regional geologic history is not well understood.
463 The presence of shallow unloading fractures that display the same attitudes as some of the deep
464 fractures is not discarded. Nonetheless, as a deep fracture dataset was available in the area, it was
465 possible to infer that the density of possible shallow unloading fractures (developed under the
466 control of either thermal-elastic contraction during uplift or erosion) is likely marginal, as frac-
467 ture spacings are comparable in both shallow and deep intervals.

468 *5.1.3 Conceptual models*

469 In the Saint-Édouard area, the steeply-dipping fractures and BPF are assumed to be pervasive
470 throughout the sedimentary succession, from the shallow aquifers to the gas reservoir (Utica
471 Shale) and hence, throughout the intermediate zone. The F1 and F2 sets are orthogonal to each
472 other and to the bedding planes. F1 fractures may be concentrated in corridors but this pattern
473 remains to be confirmed. F1 and F2 fracture sets are also present in siltstone units and observa-
474 tions on outcrops showed that these sets are more homogeneously distributed in this unit (similar
475 F1 and F2 spacing values). A third fracture set (F3) was observed in the Utica Shale and locally
476 in the Lorraine Group, where these fractures are more sparsely distributed. A fourth set, corre-
477 sponding to BPF, was only observed in shallow shale units within the upper 60 m of bedrock.
478 The observation of BPF was easier at shallow depth because their aperture is enhanced in this

interval, probably as a consequence of glaciations/de-glaciations events or de-compaction in a context of erosion and uplift. However, some BPF should exist at depth in the study area as in many other shale successions (Gale et al., 2015; Gale et al., 2016; Wang and Gale, 2016).

A conceptual model integrating all the elements acquired about the fracture pattern affecting the sedimentary succession of the Saint-Édouard area is proposed in Fig. 16. Schematics of the fracture network were developed using two scales to better represent their characteristics and features: the mesoscale (1 km blocks in Fig. 16a, b and c) and the metric (local) scale (Fig. 16d and e). The size of the metric scale blocks corresponds to the representative elementary volume (REV) of the fracture network that affects each lithological unit (shale or siltstone). A REV is defined as the minimum volume of sampling domains beyond which its characteristics remain constant (Bear, 1972). The REV properties could be used to further explore the hydraulic controls of this fracture network in numerical models with a Discrete Fracture Networks (DFN) approach. For stratabound fractures, such as those in the siltstone units, the size of the REV (a metric scale block) should be at least one or two times larger than the mean fracture spacing (Odling et al., 1999). Thus, for the highly fractured siltstone units, a REV of 0.5 m size can be defined (Fig. 16e). For non-stratabound systems, such as in the shale units, it is recommended to define a REV larger than the maximum mean trace length of fractures (Voeckler, 2012); in fact, a size at least three times larger than the mean trace is suggested (Oda, 1985, 1988). The approximate maximum mean fracture length observed in shale units is 5 m. For this reason, a 15 m long REV is proposed (Fig. 16d). However, due to the lack of large outcropping areas in the Saint-Édouard area, more fracture length measurements would be recommended in neighbouring areas for a finer estimation of the REV dimensions in shale units. It must be kept in mind that these REV are theoretical volumes that could not exist in the field due to the complexity and continuity of

fluid flow circulation in the fracture network (Kulatilake and Panda, 2000; Neuman, 1988). However, in a context of low porosity and permeability rock in the SLP (BAPE 2010; Séjourné, 2015; Séjourné et al., 2013), fluid circulation can only be envisioned through open fractures and very little within the matrix. Therefore, the definition of a REV is simply a first step to better assess the control of fractures on fluid flow.

Insert fig. 16 here.

5.2 *Implications for the assessment of potential upward fluid migration*

5.2.1 Limits of the conceptual model

In the Saint-Édouard area, the caprock and shale gas reservoir are affected by several fracture sets that are pervasive throughout the region and the entire stratigraphic succession. The experimental variograms showed that fractures are clustered and the parameters extracted from semi-variograms could be used for other studies to generate simulation of stochastic fracture networks fracture (in DFN models for example). Scale-dependant change in structure, such as the existence of fracture corridors, could not be identified using these variogram as this approach assumes that fracture spacing is a scale-independent continuous variable. As a consequence to further assess the heterogeneity of this fracture pattern, gains could be obtained by the use of parameters such as lacunarity which describes the scale-dependant changes in fracture patterns (Roy, 2013; Roy et al., 2014). For the specific case of the Saint-Édouard area, more field data would be necessary to rigorously document this entire range of heterogeneity. At regional scale, the progressive deepening of the platform to the southeast may also have had a control on small

524 and large scale fracturing but it could not be confirmed with the existing datasets in the studied
525 area.

526 In addition, the outcropping areas were limited in size and number and borehole data cannot pro-
527 vide any direct observation of fracture lengths. As a consequence, the vertical extension of frac-
528 tures, and thus the vertical continuity of the fracture network between the deep gas reservoir and
529 shallow aquifers cannot be undoubtedly determined solely based on the currently available struc-
530 tural datasets. This highlights the limits of using analogs when regarding to the potential exist-
531 ence of large-scale preferential fluid flow pathways in a sedimentary succession. However, the
532 approach is particularly useful in fracture network characterisation studies, to make up for the
533 frequent lack of data in some specific geological intervals.

534 *5.2.2 New insights for the assessment of potential upward fluid migration*

535 As direct observations of the vertical extent of structural discontinuities are challenged by the
536 limits of the available datasets and methods, data from other fields should be acquired to assess
537 the potential of upward fluid migration through the caprock. For instance, isotopic signatures of
538 gas in both rock and groundwater would provide good indicators to identify a potential hydraulic
539 connection between the deep reservoir and the surficial aquifers. In addition, the assessment of
540 the geomechanical properties of the different units within the intermediate zone would provide
541 evidence of the presence or absence of ductile strata that would control the fracture length. To
542 further explore the hydraulic controls imposed by the presence of fractures and faults, one should
543 also consider the four following points: 1) the role of individual fractures on fluid flow and espe-
544 cially their aperture throughout the stratigraphy; 2) the existence of open fractures associated
545 with regional-scale structural discontinuities, such as fault damage zones; 3) the evaluation of
546 hydraulic properties of these regional-scale features; 4) the driving mechanisms that would sup-

port upward fluid flow in these pathways (if any) throughout the entire stratigraphic succession (deep shale gas reservoir, intermediate zone and shallow aquifers).

6 Conclusion

The natural fracture pattern in both the shallow aquifers and the deep shale gas reservoir of the Saint-Édouard area was characterized using a combination of fracture data from outcrops and well logs (acoustic, optical and micro-resistivity). Three steeply-dipping fracture sets, as well as bedding-parallel fractures were documented. The three high-angle fracture sets are common to both shallow and deep units with similar characteristics such as fracture attitude and spacing. For this reason and based on the regional geologic history, these fracture sets could be used as analogs for those within the intermediate zone for which little to no data were available. These fracture sets are pervasive throughout the region, but they are heterogeneously distributed. Conceptual models of the fracture pattern were developed at metric to kilometric scales. Nonetheless, due to the limitations of the observation methods and the near absence of data for the intermediate zone, the vertical extension of natural fractures, which represents a critical parameter for aquifer vulnerability, still remains elusive. The comprehensive assessment of the caprock integrity should also be based on geomechanical properties of the different caprock units, on gas and groundwater geochemistry to provide evidence for potential upward migration and on the definition of potential hydraulic properties of fractures, fault planes and associated damage zones identified in the Saint-Édouard area, as well as their *in situ* hydrological conditions.

This paper highlighted the benefits of combining datasets from the shallow and deep intervals in fracture network characterization. It also pointed out the limitations of using analogs to assess the potential impacts of shale gas activities on shallow fresh groundwater. Even if these results

569 are strictly valid for the Saint-Édouard area, the methodology used to characterize the fracture
570 network in the caprock interval using geoscience data from the shallow and deep geological in-
571 tervals could be used in other shale gas plays where lithologies are dominated by shale units. The
572 approach could also be used in other fields, such as in geothermal energy or deep geological car-
573 bon sequestration projects, where the fracture pattern and the integrity of a rock mass relative to
574 fluid flow must be assessed.

575 **Acknowledgments**

576 This project was part of the Environmental Geoscience Program of Natural Resources Canada. It
577 also benefited from funding from the Energy Sector through the Eco-EII and PERD programs.
578 The authors wish to thank Talisman Energy (now Repsol Oil & Gas Canada) and especially Ma-
579 rianne Molgat, as well as Charles Lamontagne of the Ministère du Développement durable, de
580 l'Environnement et de la Lutte contre les Changements climatiques (MDDELCC) du Québec for
581 providing well logs data. The land owners are also thanked for the access to outcrops and drilling
582 sites. Authors are very grateful to André Guy Tranquille Temgoua, Xavier Malet and Elena Kon-
583 stantinovskaya for field support. Authors wish to thank Nicolas Pinet for his careful review of
584 the manuscript and relevant comments. Erwan Gloaguen is also thanked for his helpful com-
585 ments. The manuscript was improved by comments and suggestions from William M Dunne and
586 an anonymous reviewer. This paper is GSC contribution 20170287.

References

Antonellini, M., Mollema, P.N., 2000. A natural analog for a fractured and faulted reservoir in dolomite: Triassic Sella Group, northern Italy. AAPG Bulletin 84, 314-344.

Bai, T., Pollard, D.D., 2000. Fracture spacing in layered rocks: a new explanation based on the stress transition. Journal of Structural Geology 22, 43-57.

Bai, T., Pollard, D.D., Gao, H., 2000. Explanation for fracture spacing in layered materials. Nature 403, 753-756.

BAPE, 2010. Comparaison des shales d'Utica et de Lorraine avec des shales en exploitation, Réponse de la l'APGQ aux questions de la Commission du BAPE sur les gaz de schiste. Available at: http://www.bape.gouv.qc.ca/sections/mandats/Gaz_de_schiste/documents/DB25%20tableau%20de%20shales.pdf (accessed february 2017). Bureau d'Audiences Publiques sur l'Environnement (BAPE) DB25.

Barton, A., Hickman, S., Morin, R., 1998. Reservoir-Scale fracture permeability in the Dixie Valley, Nevada, geolthermal field Twenty-Third Workshop on Geothermal Reservoir Engineering SGP-TR-158, 299-306.

Bear, J., 1972. Dynamics of fluids in porous media. Dover Publications, inc., New York.

Belt, E.S., Riva, J., Bussières, L., 1979. Revision and correlation of late Middle Ordovician stratigraphy northeast of Quebec City. Canadian Journal of Earth Sciences 16, 1467-1483.

Berkowitz, B., 2002. Characterizing flow and transport in fractured geological media: A review. Advances in Water Resources 25, 861-884.

Bonnet, E., Bour, O., Odling, N.E., Davy, P., Main, I., Cowie, P., Berkowitz, B., 2001. Scaling of fracture systems in geological media. Reviews of Geophysics - AGU 39, 3.

Caine, J.S., Tomusiak, S.R.A., 2003. Brittle structures and their role in controlling porosity and permeability in a complex Precambrian crystalline-rock aquifer system in the Colorado Rocky Mountain Front Range. Geological Society of America Bulletin 115, 1410-1424.

Castonguay, S., Dietrich, J., Lavoie, D., Laliberté, J.-Y., 2010. Structure and petroleum plays of the St. Lawrence Platform and Appalachians in southern Quebec: insights from interpretation of MRNQ seismic reflection data. Bulletin of Canadian Petroleum Geology 58, 219-234.

Castonguay, S., Dietrich, J., Shinduke, R., Laliberté, J.-Y., 2006. Nouveau regard sur l'architecture de la Plate-forme du Saint-Laurent et des Appalaches du sud du Québec par le retraitement des profils de sismique réflexion M-2001, M-2002 et M-2003. Commission géologique du Canada, Dossier Public 5328, 19.

Castonguay, S., Séjourné, S., Dietrich, J., 2003. The Appalachian structural front in southern Quebec: Seismic and field evidence for complex structures and a triangle zone at the edge of the foreland thrust belt:. First annual joint meeting of the Geological Society of America – Northeastern Section and the Atlantic Geoscience Society, Halifax 2003, On line: http://gsa.confex.com/gsa/2003NE/finalprogram/abstract_51232.htm.

Castonguay, S.b., Ruffet, G., Tremblay, A., F ├⌐raud, G., 2001. Tectonometamorphic evolution of the Southern Quebec Appalachians: 40Ar/39 Ar evidence for Middle Ordovician crustal thickening and Silurian-Early Devonian exhumation of the internal Humber zone. 113, 144-160.

626 CCA, 2014. Environmental impacts of shale gas extraction in Canada. Available at
627 http://www.scienceadvice.ca/uploads/eng/assessments%20and%20publications%20and%20news%20rel
628 eases/shale%20gas/shalegas_fullreporten.pdf (accessed february 2017). Council of Canadian
629 Academies (CCA), 292.

630 Chilès, J., 1988. Fractal and geostatistical methods for modeling of a fracture network. Mathematical
631 Geology 20, 631-654.

632 Clark, T.H., Globensky, Y., 1973. Portneuf et parties de St-Raymond et de Lyster - Comtés de Portneuf et
633 de Lotbinière. Ministère des Richesses Naturelles, Direction Générale des Mines, Rapport Géologique
634 148.

635 Clark, T.H., Globensky, Y., 1976. Région de Bécancour. 165.

636 Comeau, F.A., Kirkwood, D., Malo, M., Asselin, E., Bertrand, R., 2004. Taconian mélanges in the
637 parautochthonous zone of the Quebec Appalachians revisited: implications for foreland basin and thrust
638 belt evolution. Canadian Journal of Earth Sciences 41, 1473-1490.

639 Crow, H.L., Ladevèze, P., 2015. Downhole geophysical data collected in 11 boreholes near St.-Édouard-
640 de-Lotbinière, Québec. Geological Survey of Canada, Open File 7768, 48.

641 Dershowitz, B., LaPointe, P., Eiben, T., Wei, L., 1998. Integration of Discrete Feature Network Methods
642 with Conventional Simulator Approaches. Society of Petroleum Engineers SPE-49069-MS.

643 Dietrich, J., Lavoie, D., Hannigan, P., Pinet, N., Castonguay, S., Giles, P., Hamblin, A.P., 2011.
644 Geological setting and resource potential of conventional petroleum plays in Paleozoic basins in eastern
645 Canada. Bulletin of Canadian Petroleum Geology 59, 54-84.

646 Ding, W., Li, C., Li, C., Xu, C., Jiu, K., Zeng, W., Wu, L., 2012. Fracture development in shale and its
647 relationship to gas accumulation. Geoscience Frontiers 3, 97-105.

648 Engelder, T., 1985. Loading paths to joint propagation during a tectonic cycle: an example from the
649 Appalachian Plateau, U.S.A. Journal of Structural Geology 7, 459-476.

650 English, J.M., 2012. Thermomechanical origin of regional fracture systems. AAPG Bulletin 96, 1597-1625.

651 EPA, 2016. Hydraulic Fracturing for Oil and Gas: Impacts from the Hydraulic Fracturing Water Cycle on
652 Drinking Water Resources in the United States (Final Report). Available at: www.epa.gov/hfstudy
653 (accessed february 2017). U.S. Environmental Protection Agency (EPA), Washington, DC EPA/600/R-
654 16/236F, 666.

655 Escuder Viruete, J., Carbonell, R., Jurado, M.J., Martí, D., Pérez-Estaún, A., 2001. Two-dimensional
656 geostatistical modeling and prediction of the fracture system in the Albala Granitic Pluton, SW Iberian
657 Massif, Spain. Journal of Structural Geology 23, 2011-2023.

658 Faure, S., Tremblay, A., Malo, M., 2004. Reconstruction of Taconian and Acadian paleostress regimes in
659 the Quebec and northern New Brunswick Appalachians. Canadian Journal of Earth Sciences 41, 619-
660 634.

661 Fiore Allwardt, P., Bellahsen, N., Pollard, D.D., 2007. Curvature and fracturing based on global
662 positioning system data collected at Sheep Mountain anticline, Wyoming. Geosphere 3, 408-421.

663 Fisher, R., 1953. Dispersion on a Sphere. Proceedings of the Royal Society of London A: Mathematical,
664 Physical and Engineering Sciences 217, 295-305.

Gale, J., Ukar, E., Elliott, S.J., Wang, Q., 2015. Bedding-Parallel Fractures in Shales: Characterization, Prediction and Importance, AAPG Annual Convention and Exhibition, Denver, CO., USA, May 31 - June 3, 2015.

Gale, J.F., Ukar, E., Wang, Q., Elliott, S.J., 2016. Bedding-Parallel Fractures in Shales, AAPG Annual Convention and Exhibition, Calgary, Alberta, Canada, June 22, 2016.

Gale, J.F.W., Laubach, S.E., Olson, J.E., Eichhubl, P., Fall, A., 2014. Natural fractures in shale: A review and new observations. AAPG Bulletin 98, 2165-2216.

Gillespie, P.A., Walsh, J.J., Watterson, J., Bonson, C.G., Manzocchi, T., 2001. Scaling relationships of joint and vein arrays from The Burren, Co. Clare, Ireland. Journal of Structural Geology 23, 183-201.

Globensky, Y., 1987. Géologie des Basses Terres du Saint-Laurent. Direction Générale de l'Exploration Géologique et minérale du Québec, Gouvernement du Québec MM 85-02.

Glorioso, J.C., Rattia, A., 2012. Unconventional reservoirs: Basic petrophysical concepts for shale gas, SPE/EAGE European Unconventional Resources Conference & Exhibition-From Potential to Production. SPE, Vienna, Austria.

Grieser, W.V., Bray, J.M., 2007. Identification of Production Potential in Unconventional Reservoirs, Production and Operations Symposium. Society of Petroleum Engineers, Oklahoma City, Oklahoma, U.S.A. .

Gross, M.R., 1993. The origin and spacing of cross joints: examples from the Monterey Formation, Santa Barbara Coastline, California. Journal of Structural Geology 15, 737-751.

Guerriero, V., Mazzoli, S., Iannace, A., Vitale, S., Carravetta, A., Strauss, C., 2013. A permeability model for naturally fractured carbonate reservoirs. Marine and Petroleum Geology 40, 115-134.

Haeri-Ardakani, O., Sanei, H., Lavoie, D., Chen, Z., Jiang, C., 2015. Geochemical and petrographic characterization of the Upper Ordovician Utica Shale, southern Quebec, Canada. International Journal of Coal Geology 138, 83-94.

Hamblin, A.P., 2006. The “Shale Gas” concept in Canada: a preliminary inventory of possibilities. Geological Survey of Canada, Open File 5389, 103.

Heidbach, O., Tingay, M., Barth, A., Reinecker, J., Kurfeß, D., Müller, B., 2009. The World Stress Map, in: 2008, S.E.b.o.t.W.d.r. (Ed.). Helmholtz Centre Potsdam - GFZ German Research Centre for Geosciences, Commission de la Carte Géologique du Monde / Commission for the Geological Map of the World.

Héroux, Y., Bertrand, R., 1991. Maturation thermique de la matière organique dans un bassin du Paléozoïque inférieur, Basses-Terres du Saint-Laurent, Québec, Canada. Canadian Journal of Earth Sciences 28, 1019-1030.

Ji, S., Saruwatari, K., 1998. A revised model for the relationship between joint spacing and layer thickness. Journal of Structural Geology 20, 1495-1508.

Konstantinovskaya, E., Malo, M., Castillo, D.A., 2012. Present-day stress analysis of the St. Lawrence Lowlands sedimentary basin (Canada) and implications for caprock integrity during CO2 injection operations. Tectonophysics 518-521, 119-137.

703 Konstantinovskaya, E., Rodriguez, D., Kirkwood, D., Harris, L., Thériault, R., 2009. Effects of basement
704 structure, sedimentation and erosion on thrust wedge geometry: an example from the Quebec
705 Appalachians and analogue models. Bulletin of Canadian Petroleum Geology 57, 34-62.

706 Kulatilake, P.H.S.W., Panda, B.B., 2000. Effect of Block Size and Joint Geometry on Jointed Rock
707 Hydraulics and REV. Journal of Engineering Mechanics 126.

708 Ladeira, F.L., Price, N.J., 1981. Relationship between fracture spacing and bed thickness. Journal of
709 Structural Geology 3, 179-183.

710 Lai, J., Wang, G., Huang, L., Li, W., Ran, Y., Wang, D., Zhou, Z., Chen, J., 2015. Brittleness index
711 estimation in a tight shaly sandstone reservoir using well logs. Journal of Natural Gas Science and
712 Engineering 27, Part 3, 1536-1545.

713 Larsen, B., Grunnaleite, I., Gudmundsson, A., 2010. How fracture systems affect permeability
714 development in shallow-water carbonate rocks: An example from the Gargano Peninsula, Italy. Journal of
715 Structural Geology 32, 1212-1230.

716 Laubach, S.E., Olson, J.E., Gross, M.R., 2009. Mechanical and fracture stratigraphy. AAPG Bulletin 93,
717 1413-1426.

718 Lavenu, A.P., Lamarche, J., Gallois, A., Gauthier, B.D., 2013. Tectonic versus diagenetic origin of
719 fractures in a naturally fractured carbonate reservoir analog (Nerthe anticline, southeastern France).
720 AAPG Bulletin 97, 2207-2232.

721 Lavoie, D., 2008. Chapter 3 Appalachian Foreland Basin of Canada, in: Andrew, D.M. (Ed.), Sedimentary
722 Basins of the World. Elsevier, pp. 65-103.

723 Lavoie, D., Desrochers, A., Dix, G., Knight, I., Salad Hersi, O., 2012. The Great American Carbonate
724 Bank in Eastern Canada: An Overview. In: Derby, J.R., Fritz, R.D., Longacre, S.A., Morgan, W.A.,
725 Sternbach, C.A. (Eds.), The Great American Carbonate Bank. The Geology and Economic Resources of
726 the Cambrian–Ordovician Sauk Megasequence of Laurentia. AAPG Memoirs 98, 499-523.

727 Lavoie, D., Hamblin, A.P., Theriault, R., Beaulieu, J., Kirkwood, D., 2008. The Upper Ordovician Utica
728 Shales and Lorraine Group flysch in southern Québec: Tectonostratigraphic setting and significance for
729 unconventional gas. Commission géologique du Canada, Open File 5900, 56.

730 Lavoie, D., Pinet, N., Bordeleau, G., Ardakani, O.H., Ladevèze, P., Duchesne, M.J., Rivard, C., Mort, A.,
731 Brake, V., Sanei, H., Malet, X., 2016. The Upper Ordovician black shales of southern Quebec (Canada)
732 and their significance for naturally occurring hydrocarbons in shallow groundwater. International Journal
733 of Coal Geology 158, 44-64.

734 Lavoie, D., Rivard, C., Lefebvre, R., Séjourné, S., Thériault, R., Duchesne, M.J., Ahad, J.M.E., Wang, B.,
735 Benoit, N., Lamontagne, C., 2014. The Utica Shale and gas play in southern Quebec: Geological and
736 hydrogeological syntheses and methodological approaches to groundwater risk evaluation. International
737 Journal of Coal Geology 126, 77-91.

738 Lefebvre, R., 2016. Mechanisms leading to potential impacts of shale gas development on groundwater
739 quality. Wiley Interdisciplinary Reviews: Water, n/a-n/a.

740 McConaughy, D.T., Engelder, T., 1999. Joint interaction with embedded concretions: joint loading
741 configurations inferred from propagation paths. Journal of Structural Geology 21, 1637-1652.

742 Meng, F., Zhou, H., Zhang, C., Xu, R., Lu, J., 2015. Evaluation Methodology of Brittleness of Rock Based
743 on Post-Peak Stress–Strain Curves. Rock Mech Rock Eng 48, 1787-1805.

744 Miller, S.M., 1979. Determination of spatial dependence in fracture set characteristics by geostatistical
745 methods, Department of mining and geological engineering. The University of Arizona, p. 122.

746 Min, K.-B., Jing, L., Stephansson, O., 2004. Determining the equivalent permeability tensor for fractured
747 rock masses using a stochastic REV approach: Method and application to the field data from Sellafield,
748 UK. Hydrogeology Journal 12, 497-510.

749 Mozley, P.S., Davis, J.M., 2005. Internal structure and mode of growth of elongate calcite concretions:
750 Evidence for small-scale, microbially induced, chemical heterogeneity in groundwater. Geological Society
751 of America Bulletin 117, 1400-1412.

752 Narr, W., Schechter, D.W., Thompson, L.B., 2006. Naturally fractured reservoir characterization.
753 Richardson, TX: Society of Petroleum Engineers.

754 Narr, W., Suppe, J., 1991. Joint spacing in sedimentary rocks. Journal of Structural Geology 13, 1037-
755 1048.

756 Neuman, S.P., 1988. Stochastic Continuum Representation of Fractured Rock Permeability as an
757 Alternative to the REV and Fracture Network Concepts, in: Custodio, E., Gurgui, A., Ferreira, J.P.L.
758 (Eds.), Groundwater Flow and Quality Modelling. Springer Netherlands, Dordrecht, pp. 331-362.

759 Oda, M., 1985. Permeability tensor for discontinuous rock masses. Geotechnique 35, 483-495.

760 Oda, M., 1988. A method for evaluating the representative elementary volume based on joint survey of
761 rock masses. Canadian Geotechnical Journal 25, 440-447.

762 Odling, N.E., Gillespie, P., Bourgine, B., Castaing, C., Chiles, J.P., Christensen, N.P., Fillion, E., Genter,
763 A., Olsen, C., Thrane, L., Trice, R., Aarseth, E., Walsh, J.J., Watterson, J., 1999. Variations in fracture
764 system geometry and their implications for fluid flow in fractures hydrocarbon reservoirs. Petroleum
765 Geoscience 5, 373-384.

766 Ogunyomi, O., Hesse, R., Heroux, Y., 1980. Pre-Orogenic and Synorogenic Diagenesis and
767 Anchimetamorphism in Lower Paleozoic Continental Margin Sequences of the Northern Appalachians in
768 and Around Quebec City, Canada. Bulletin of Canadian Petroleum Geology 28, 559-577.

769 Park, H.J., West, T.R., 2002. Sampling bias of discontinuity orientation caused by linear sampling
770 technique. Engineering Geology 66, 99-110.

771 Pinet, N., 2011. Deformation in the Utica Shale and Lorraine Group, Saint Lawrence Lowlands, Québec.
772 Geological Survey of Canada, Open File 6952, 12.

773 Pinet, N., Duchesne, M., Lavoie, D., Bolduc, A.e., Long, B., 2008. Surface and subsurface signatures of
774 gas seepage in the St. Lawrence Estuary (Canada): Significance to hydrocarbon exploration. Marine and
775 Petroleum Geology 25, 271-288.

776 Pinet, N., Lavoie, D., Keating, P., Duchesne, M., 2014. The St Lawrence Platform and Appalachian
777 deformation front in the St Lawrence Estuary and adjacent areas (Quebec, Canada): structural complexity
778 revealed by magnetic and seismic imaging. Geological Magazine 151, 996-1012.

779 Rivard, C., Lavoie, D., Lefebvre, R., Séjourné, S., Lamontagne, C., Duchesne, M., 2014. An overview of
780 Canadian shale gas production and environmental concerns. International Journal of Coal Geology 126,
781 64-76.

782 Roy, A., 2013. Scale-dependent heterogeneity in fracture data sets and grayscale images. The University
783 of Tennesee.

784 Roy, A., Perfect, E., Dunne, W.M., McKay, L.D., 2014. A technique for revealing scale-dependent
785 patterns in fracture spacing data. Journal of Geophysical Research: Solid Earth 119, 5979-5986.

786 Sasseville, C., Clauer, N., Tremblay, A., 2012. Timing of fault reactivation in the upper crust of the St.
787 Lawrence rift system, Canada, by K–Ar dating of illite-rich fault rocks1. Canadian Journal of Earth
788 Sciences 49, 637-652.

789 Sasseville, C., Tremblay, A., Clauer, N., Liewig, N., 2008. K–Ar age constraints on the evolution of
790 polydeformed fold–thrust belts: The case of the Northern Appalachians (southern Quebec). Journal of
791 Geodynamics 45, 99-119.

792 Séjourné, S., 2015. Caractérisation des réseaux de fractures naturelles, de la porosité et de la saturation
793 en eau du Shale d'Utica et de sa couverture par l'analyse des diagraphies de forages pétroliers dans la
794 région de Saint-Édouard, Québec. Commission Géologique du Canada, Dossier Public 7980, 60.

795 Séjourné, S., 2017. Étude géomécanique du Shale d'Utica et de sa couverture d'après les puits pétroliers
796 et gaziers de la région de Saint-Édouard-de-Lotbinière, Québec. Commission Géologique du Canada,
797 Dossier Public 8196, 54.

798 Séjourné, S., Dietrich, J., Malo, M., 2003. Seismic characterization of the structural front of southern
799 Quebec Appalachians. Bulletin of Canadian Petroleum Geology 51, 29-44.

800 Séjourné, S., Lefebvre, R., Malet, X., Lavoie, D., 2013. Synthèse géologique et hydrogéologique du Shale
801 d'Utica et des unités sus-jacentes (Lorraine, Queenston et dépots meubles), Basses-Terres du Saint-
802 Laurent, Québec. Commission Géologique du Canada, Dossier Public 7338, 165.

803 Sikander, A., Pittion, J., 1978. Reflectance studies on organic matter in lower Paleozoic sediments of
804 Quebec. Bulletin of Canadian Petroleum Geology 26, 132-151.

805 Singhal, B.B.S., Gupta, R.P., 2010. Applied Hydrogeology of Fractured Rocks. Springer Netherlands.

806 St-Julien, P., Hubert, C., 1975. Evolution of the Taconian orogen in the Quebec Appalachians. American
807 Journal of Science 275-A, 337-362.

808 St-Julien, P., Slivitsky, A., Feininger, T., 1983. A deep structural profile across the Appalachians of
809 southern Quebec. Geological Society of America Memoirs 158, 103-112.

810 Stesky, M., 2010. Pangea Scientific - Spheristat Version 3.1 - User's Manual.

811 Surrette, M., Allen, D.M., Journeay, M., 2008. Regional evaluation of hydraulic properties in variably
812 fractured rock using a hydrostructural domain approach. Hydrogeology Journal 16, 11-30.

813 Tavchandjian, O., Rouleau, A., Archambault, G., Daigneault, R., Marcotte, D., 1997. Geostatistical
814 analysis of fractures in shear zones in the Chibougamau area: applications to structural geology.
815 Tectonophysics 269, 51-63.

816 Terzaghi, R.D., 1965. Sources of error in joint surveys. Geotechnique 15 (3), 287-304.

817 Theriault, R., 2012. Caractérisation du Shale d'Utica et du Groupe de Lorraine, Basses-Terres du Saint-
818 Laurent - Partie 2 : Interprétation Géologique, in: Québec, M.d.R.N.e.F. (Ed.), p. 80.

819 Thériault, R., 2007. Trenton/Black River Hydrothermal Dolomite Reservoirs in Québec: The Emergence of
820 a New and Highly Promising Play along the St. Lawrence Platform. American Association of Petroleum
821 Geologists. Eastern Section Annual Meeting, Abstract with Programs 57.

822 Tremblay, A., Pinet, N., 2016. Late Neoproterozoic to Permian tectonic evolution of the Quebec
823 Appalachians, Canada. Earth-Science Reviews 160, 131-170.

824 Tremblay, A., Roden-Tice, M.K., Brandt, J.A., Megan, T.W., 2013. Mesozoic fault reactivation along the
825 St. Lawrence rift system, eastern Canada: Thermochronologic evidence from apatite fission-track dating.
826 Geological Society of America Bulletin 125, 794-810.

827 Valley, B.C., 2007. The relation between natural fracturing and stress heterogeneities in deep-seated
828 crystalline rocks at Soultz-sous-Forêts (France). Swiss Federal Institute of Technology (ETH), Zurich, p.
829 277.

830 Villaescusa, E., Brown, E.T., 1990. Characterizing joint spatial correlations using geostatistical methods,
831 in: C. A. Barton and O. Stephansson, B. (Ed.), Rock Joints.

832 Vitale, S., Dati, F., Mazzoli, S., Ciarcia, S., Guerriero, V., Iannace, A., 2012. Modes and timing of fracture
833 network development in poly-deformed carbonate reservoir analogues, Mt. Chianello, southern Italy.
834 Journal of Structural Geology 37, 223-235.

835 Voeckler, H., 2012. Modeling deep groundwater flow throught fractured bedrock in a mountainous
836 headwater catchment using a coupled surface water-groundwater model, Okanagan basin, British
837 Columbia. The University of British Columbia, Vancouver, p. 433.

838 Wang, D., Ge, H., Wang, X., Wang, J., Meng, F., Suo, Y., Han, P., 2015. A novel experimental approach
839 for fracability evaluation in tight-gas reservoirs. Journal of Natural Gas Science and Engineering 23, 239-
840 249.

841 Wang, Q., Gale, J.F., 2016. Characterizing Bedding-Parallel Fractures in Shale: Aperture-Size
842 Distributions and Spatial Organization, AAPG Annual Convention and Exhibition, Calgary, Alberta,
843 Canada, June 22, 2016.

844 Wu, H., D. Pollard, D., 1995. An experimental study of the relationship between joint spacing and layer
845 thickness. Journal of Structural Geology 17, 887-905.

846 Yang, C., Hesse, R., 1993. Diagenesis and anchimetamorphism in an overthrust belt, external domain of
847 the Taconian Orogen, southern Canadian Applachians-II. Paleogeothermal gradients derived from
848 maturation of different types of organic matter. Organic Geochemistry 20, 381-403.

849 Zoback, M.L., 1992. First- and second-order patterns of stress in the lithosphere: The World Stress Map
850 Project. Journal of Geophysical Research: Solid Earth 97, 11703-11728.
851
852

853 Table 1. List of measurement stations

Measurement station	ID	UTM coordinates (NAD83 19N)			Lithology	Group	Number of fractures	Outcrop size (approximativelly) / borehole lenght in the bedrock (m)	Outcrop or well direction (°N)
		X (m)	Y (m)	UTM Zone					
Outcrop (river bed)	1	263815	5151764	19T	Shale	Queenston	33	60	90
Outcrop (river bed)	2	263877	5152879	19T	Shale	Lorraine	49	50	120
Outcrop (river bed)	3	270891	5161970	19T	Shale	Lorraine	5	10	10
Outcrop (river bed)	4	272323	5160028	19T	Shale	Lorraine	45	15	340
Outcrop (river bed)	5	279520	5159255	19T	Shale	Lorraine	22	20	90
Outcrop (river bed)	6	278734	5169518	19T	Shale	Sainte-Rosalie	126	4 x 20	44; 120; 150; 160
Outcrop (river bed)	7	285270	5166177	19T	Shale	Lorraine	29	60	160
Outcrop (river bed)	8	289280	5167441	19T	Shale	Lorraine	29	15	10
Outcrop (vertical wall)	9	290718	5167411	19T	Siltstones	Lorraine	18	20	40
Outcrop (river bed)	10	290937	5167320	19T	Shale	Lorraine	35	50	160
Outcrop (vertical wall)	11	291434	5167412	19T	Siltstones	Lorraine	28	150	90
Outcrop (vertical wall)	12	294107	5167496	19T	Shale	Lorraine	13	20	70
Outcrop (vertical wall)	13	294715	5167631	19T	Shale	Lorraine	46	20	70
Outcrop (vertical wall)	14	294989	5167677	19T	Shale	Lorraine	7	20	70
Outcrop (river bed)	15	296619	5167487	19T	Shale	Lorraine	12	10	0
Outcrop (river bed)	16	296866	5168006	19T	Shale	Lorraine	17	50	140
Outcrop (river bed)	17	299783	5169320	19T	Shale	Sainte-Rosalie	120	2 x 20	130; 30
Shallow well	1	281370	5168963	19T	Shale	Sainte-Rosalie	10	47	vertical
Shallow well	2	287925	5155391	19T	Shale	Sainte-Rosalie	42	46	vertical
Shallow well	3	282584	5158820	19T	Shale & Siltstone	Lorraine	50	30	vertical
Shallow well	4	288214	5157504	19T	Shale	Sainte-Rosalie	39	20	vertical
Shallow well	7	276263	5164099	19T	Shale	Lorraine	19	40	vertical
Shallow well	8	277620	5162758	19T	Shale & Siltstone	Lorraine	49	50	vertical
Shallow well	10	286450	5157073	19T	Shale	Sainte-Rosalie	25	15	vertical
Shallow well	11	286396	5156776	19T	Shale	Sainte-Rosalie	19	50	vertical
Shallow well	13	286807	5156653	19T	Shale	Sainte-Rosalie	2	59	vertical
Shallow well	21	287026	5156377	19T	Shale	Sainte-Rosalie	52	148	vertical
Deep well	A	280035	5154051	19T	Shale	Sainte-Rosalie	96	424	vertical
Deep well	B	269837	5152004	19T	Shale	Sainte-Rosalie	1354	1758	vertical
Deep well	C	707892	5133892	18T	Shale	Sainte-Rosalie	812	1165	vertical
Deep well	A	280035	5154051	19T	Shale	Lorraine	56	195	vertical
Deep well	B	269837	5152004	19T	Shale	Lorraine	1325	255	vertical
Deep well	C	707892	5133892	18T	Shale	Lorraine	588	275	vertical
Horizontal well	A	280035	5154051	19T	Shale	Lorraine	2085	1020	316
Horizontal well	B	269837	5152004	19T	Shale	Lorraine	3254	600	316
Horizontal well	C	707892	5133892	18T	Shale	Lorraine	1986	950	307

854

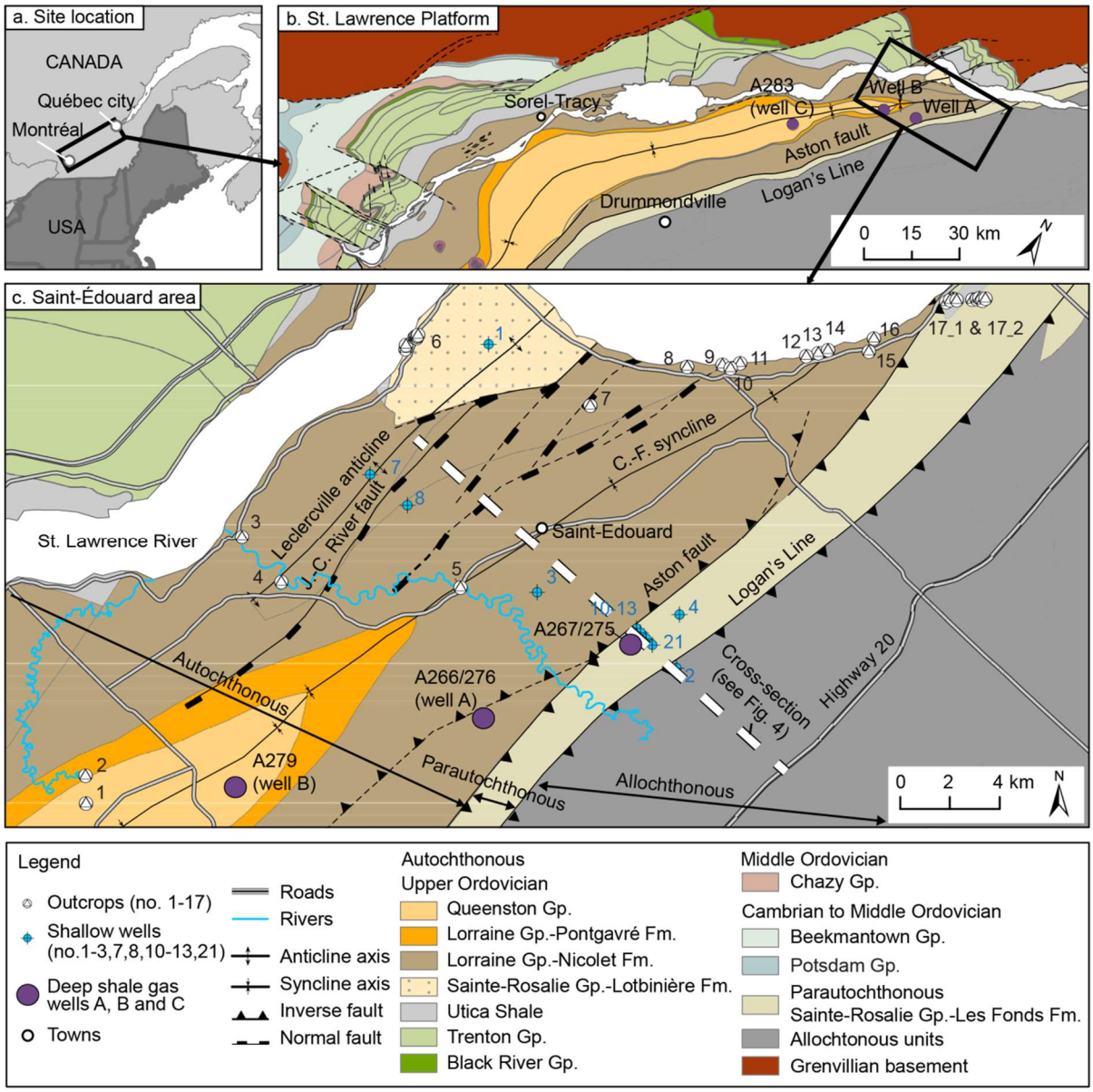

Fig. 1. The Saint-Édouard area location and its geological context: a. location of the St. Lawrence Platform; b. geological framework of the St. Lawrence Platform (modified from Globensky (1987)); c. geological map of the Saint-Édouard area (Clark and Globensky, 1973; Globensky, 1987; Lavoie et al., 2016; Thériault and Beauséjour, 2012). Faults represented as dashed lines indicate interpreted shallow faults projected from seismic data. J.-C. River fault: Jacques-

861 Cartier River fault; C.-F. syncline: Chambly-Fortierville syncline ; Gp. : Group ; Fm. : Forma-
862 tion.

863

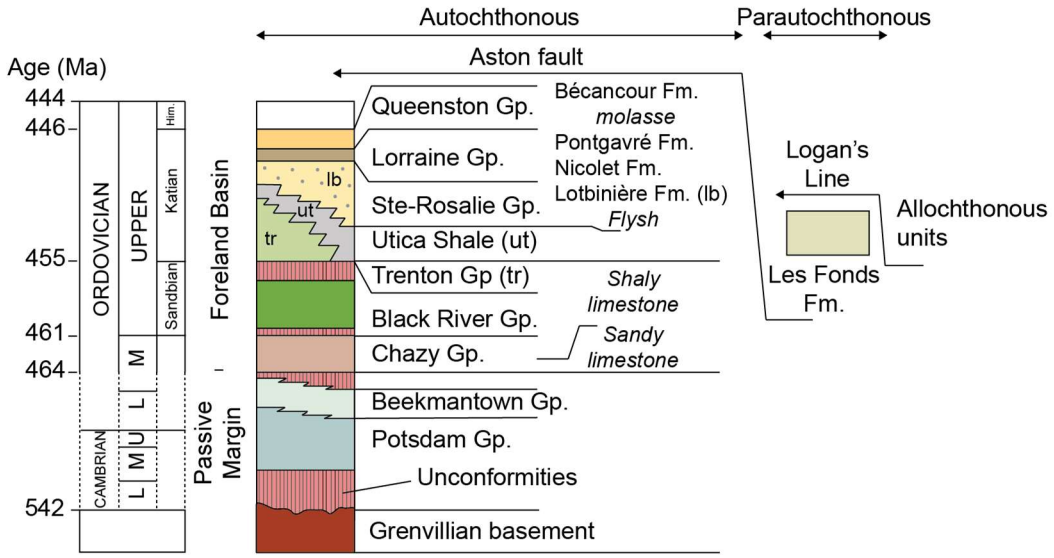

864

865 Fig. 2. Stratigraphy of the Saint-Édouard area units (modified from Konstantinovskaya et al.
866 (2014). Gp. : Group ; Fm. : Formation.

867

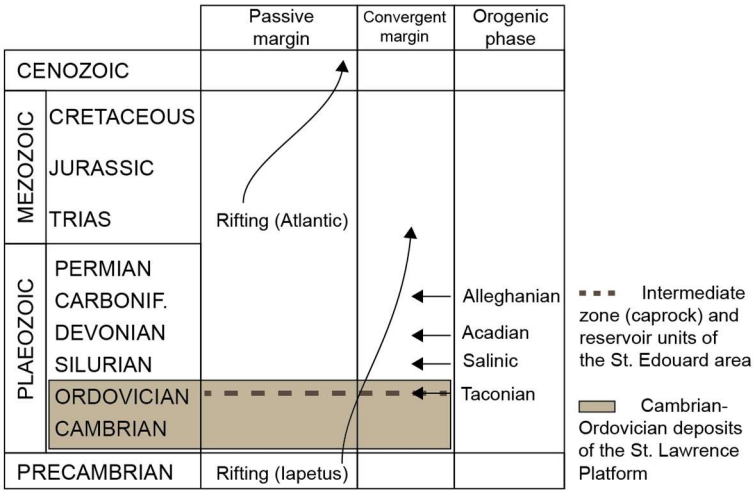

868

869 Fig. 3. Tectonic calendar recorded in the studied area, modified from Lavoie (2008).

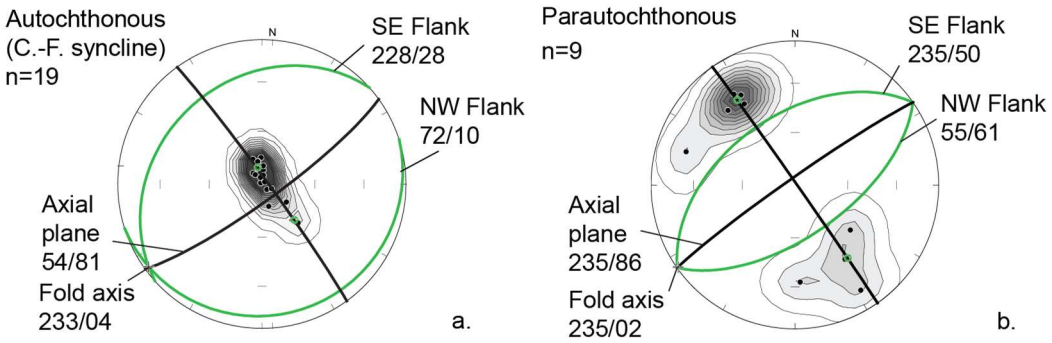

Fig. 4. Stereographic projection (lower hemisphere Schmidt stereodiagram) of the bedding plane attitudes measured in the autochthonous (a.) and parautochthonous (b.) domains. Each pole corresponds to the mean bedding plane attitude measured on each outcrop and shallow well in the Saint-Édouard area. C.F. syncline: Chambly-Fortierville syncline; n: number of measurement sites (outcrops or wells).

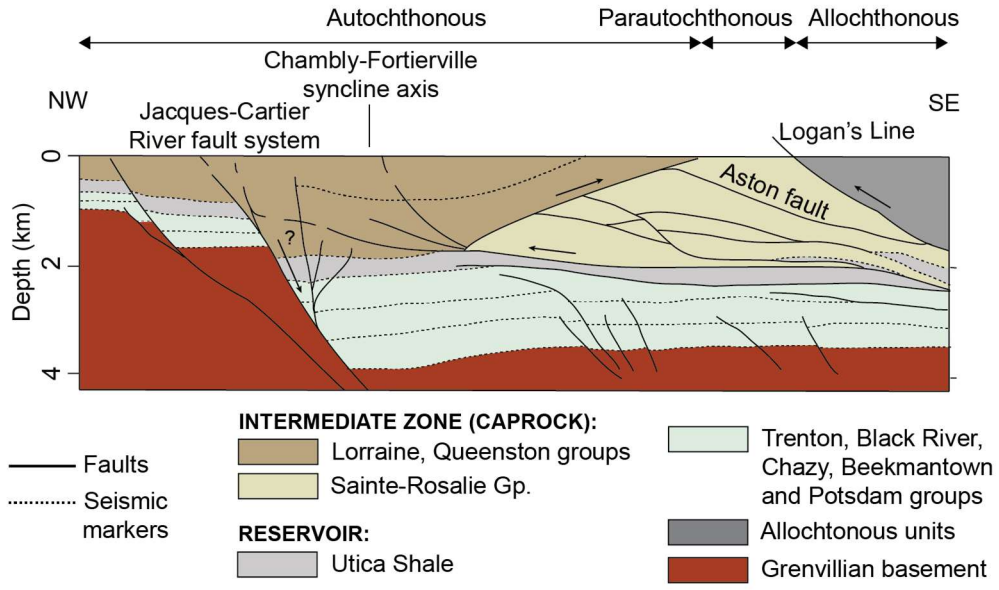

879 Fig. 5. Cross-section in the Saint-Édouard area (see Fig. 1 for location). Interpretation proposed
880 by Lavoie et al. (2016) and based on industrial seismic data. Gp: Group.

881

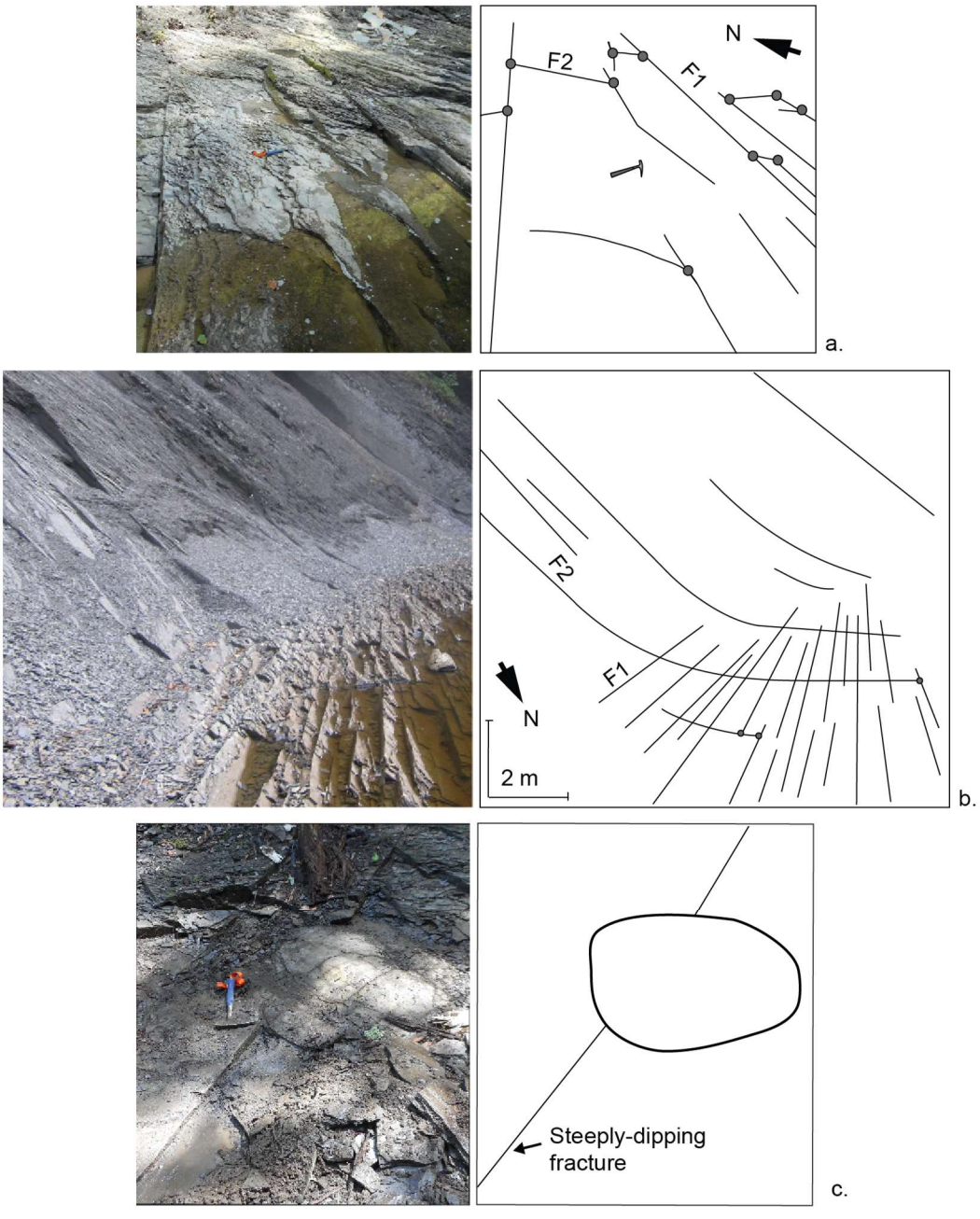

882

883 Fig. 6. Examples of fracture observations on outcropping shales: a. and b. Fracture sets 1 and 2
884 abutting relationships in the outcropping Lorraine Group (a; site 10) and Les Fonds Formations

(b; site 17). The gray dots highlight the abutting relationships between fracture sets; d. example of a fracture that abuts a calcareous concretion at site 6.

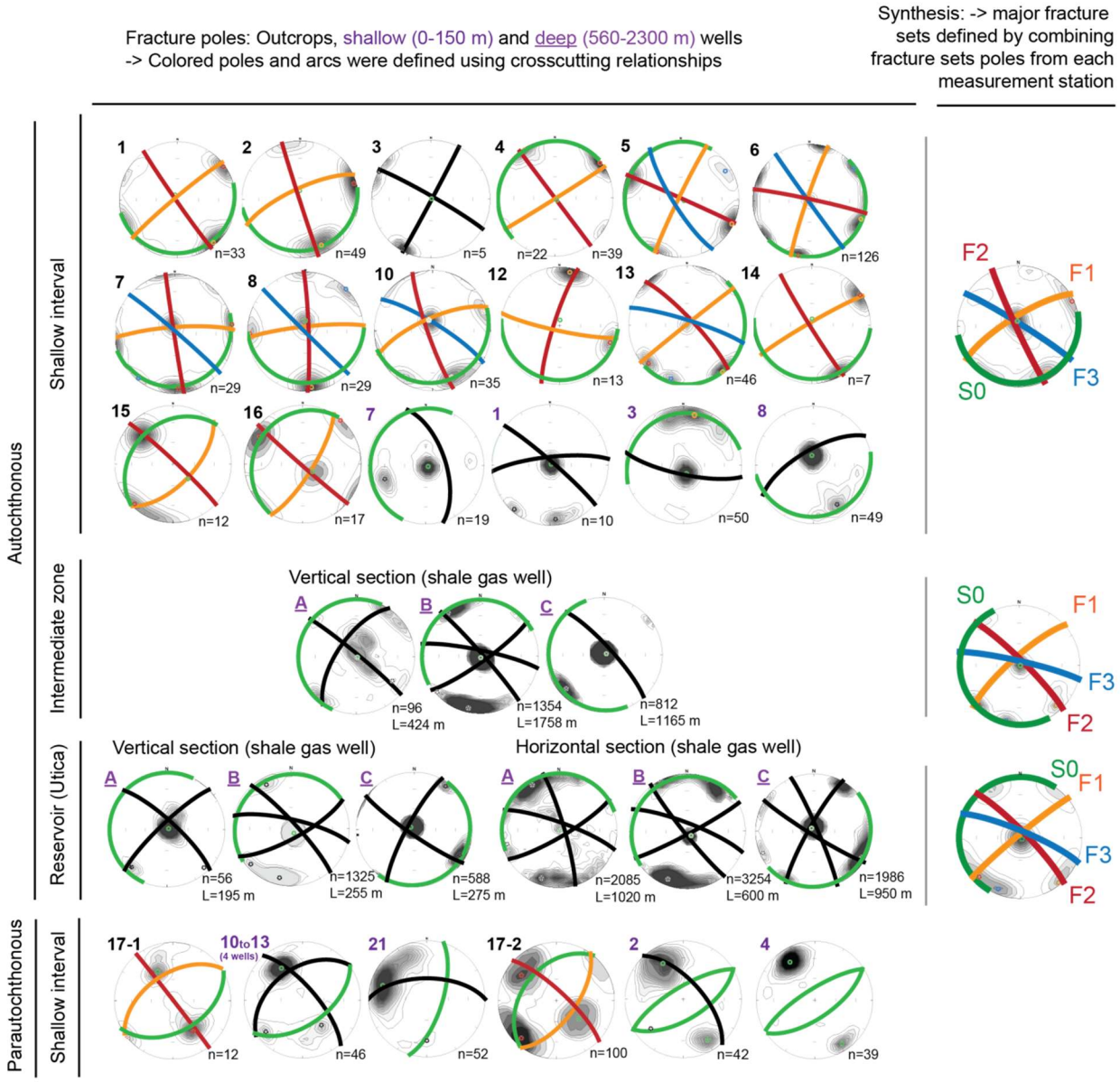

Fig. 7. Attitudes of the fracture sets identified in wells and outcrops intersecting shales in the Saint-Édouard area. The mean fracture sets and bedding planes attitudes estimated for each station are compiled in the "synthesis" stereonets. Fracture and bedding planes poles are plotted in a

lower hemisphere Schmidt representation. For outcrop data, contoured densities are not significant as they vary with the number of features measured in each outcrop (a function of the outcrop and well dimensions); densities were corrected for the sampling bias in borehole data. J.-C.: Jacques-Cartier; C.-F.: Chambly-Fortierville; n: number of fractures for each outcrop/well; L: length of the well section logged;

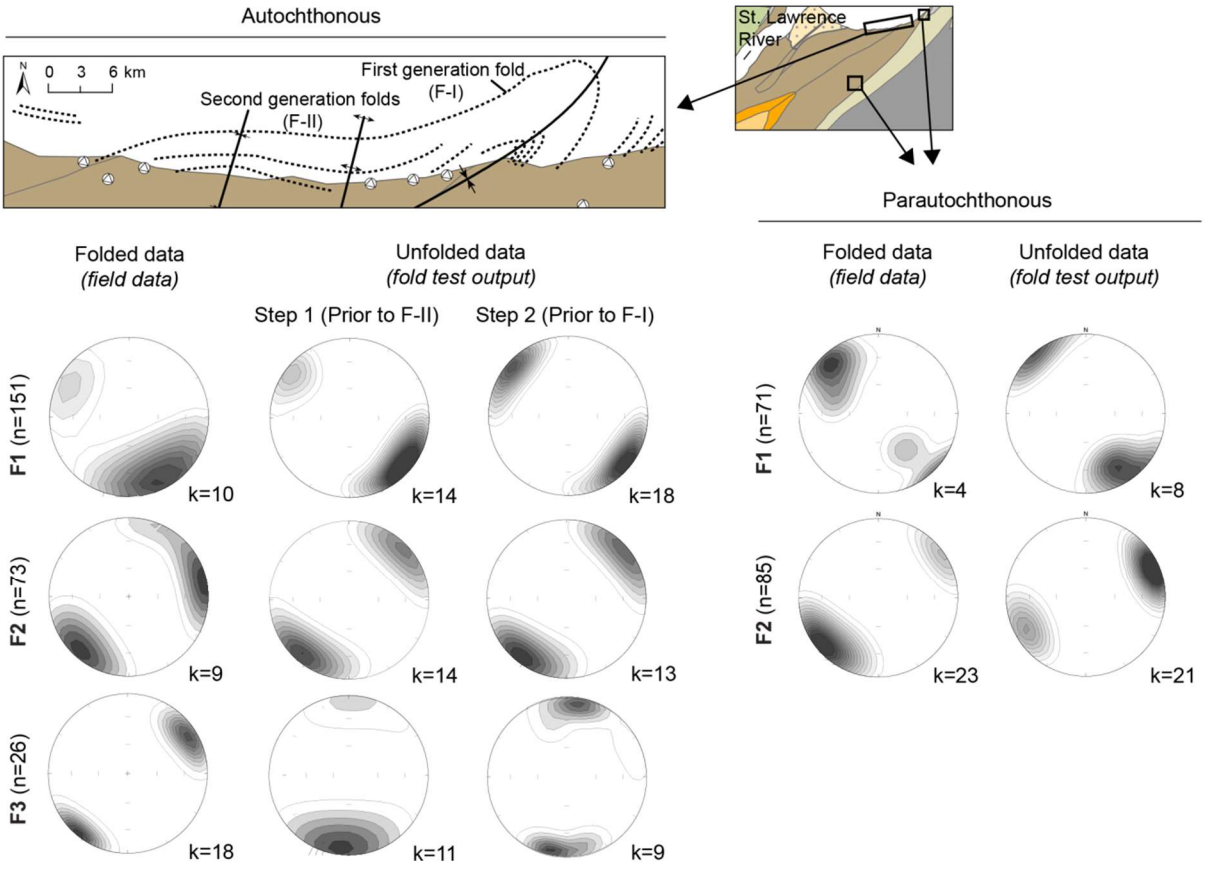

Fig. 8. Fracture attitudes variations during the fold test. The fracture data used in the analysis comes from outcrops 5 & 7 to 16 (autochthonous) and from outcrop 17 and wells #10, 11 and 13 (parautochthonous). Fault and fold axis locations presented in the maps were initially described in Clark and Globensky (1973) and Pinet (2011). F-I and F-II: first and second generations folds.

Two folds generations were identified in the autochthonous domain and one folding event was identified in the parautochthonous domain. The parameter k quantifies the degree of data concentration (higher values correspond to highly concentrated data).

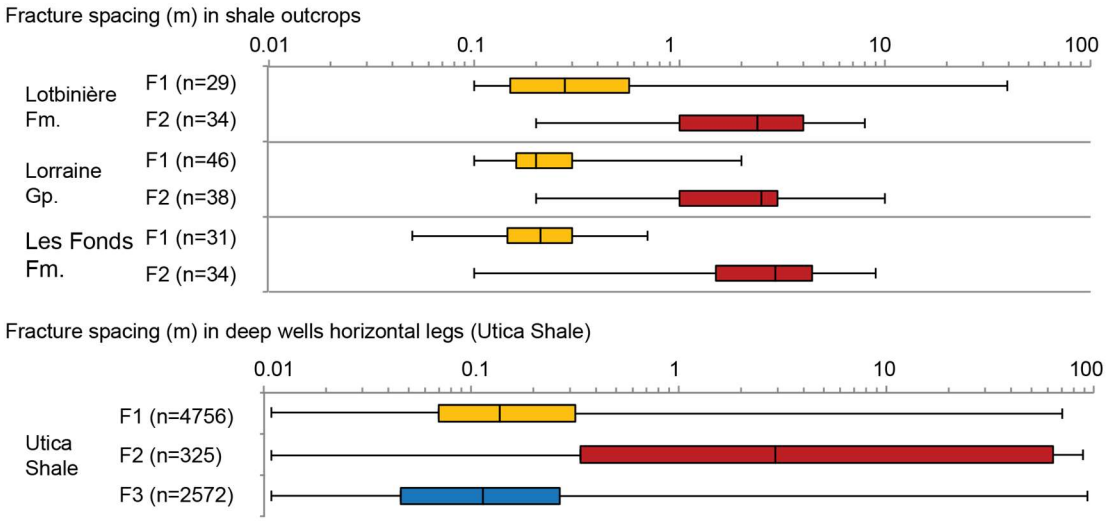

Fig. 9. Fracture spacing measured on outcrops of the Lorraine Group shale (15 sites) and in three deep well horizontal legs located in the Utica Shale. The box plot diagrams show, from right to left, maximum, upper quartile (75th percentile), median value, lower quartile (25th percentile) and minimum fracture spacing for the F1, F2 and F3 fracture sets.

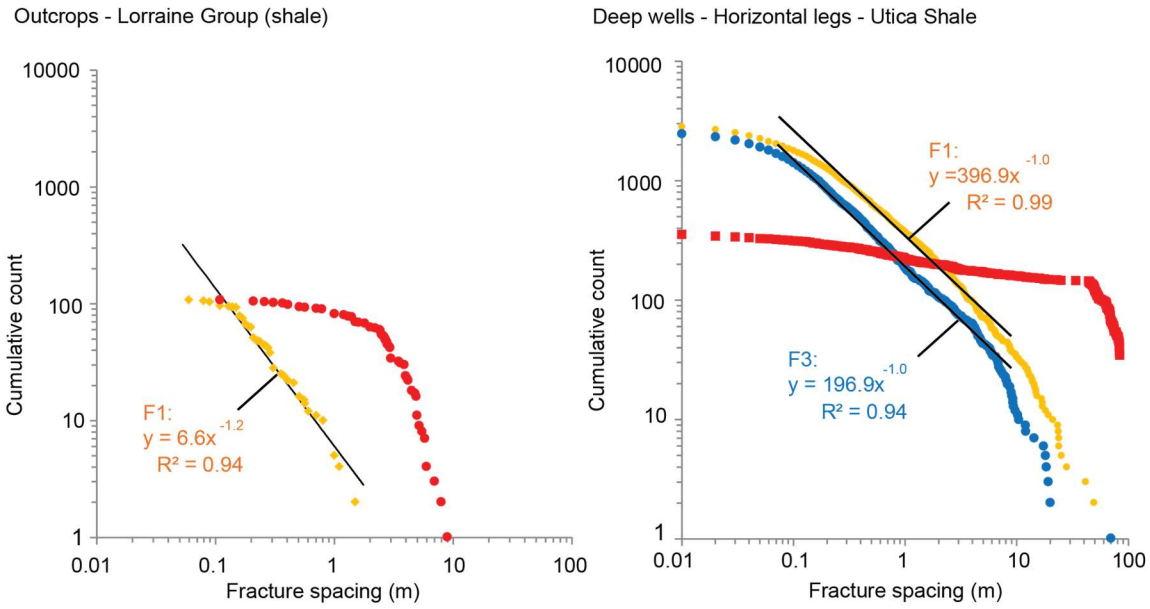

913

914 Fig. 10. Fracture spacing distributions from outcrops and deep wells. The number of F3 fracture

915 spacings measured in outcrops was insufficient to present meaningful results.

916

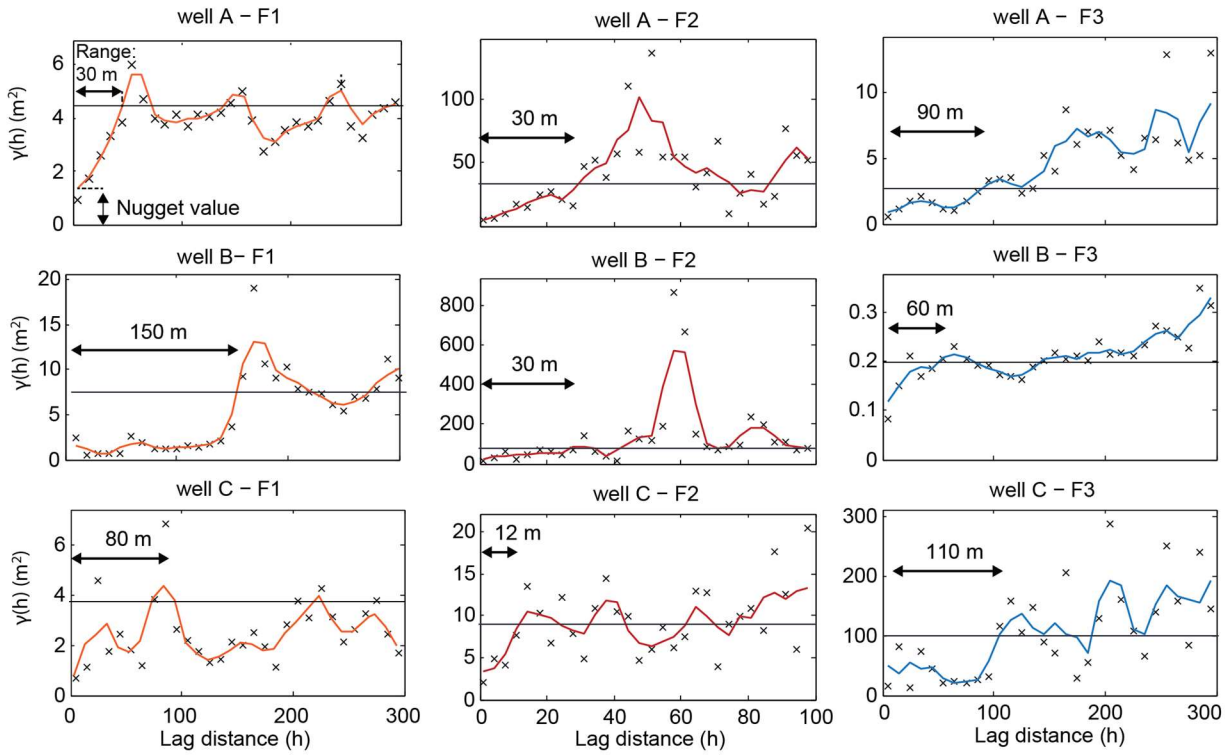

917

918 Fig. 11. Experimental variograms for spacing of fractures with respect to the distance lag h along
919 the horizontal legs of the deep wells (Utica Shale). A moving average curve was added for a bet-
920 ter identification of the trends in the calculated variograms. The horizontal line corresponds to
921 the variance of the entire fracture spacing sample. This representation highlights the limit beyond
922 which fracture spacing is not correlated (range) for F1, F2 and F3.

923

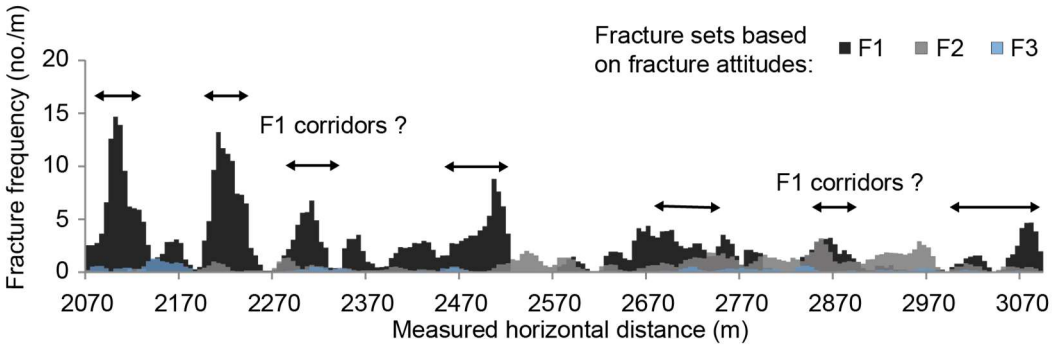

924

925 Fig. 12. Fracture densities in the horizontal leg of the deep shale gas well A (Utica Shale). Frac-
926 ture frequencies were calculated using a 20 m window length every 5 m.

927

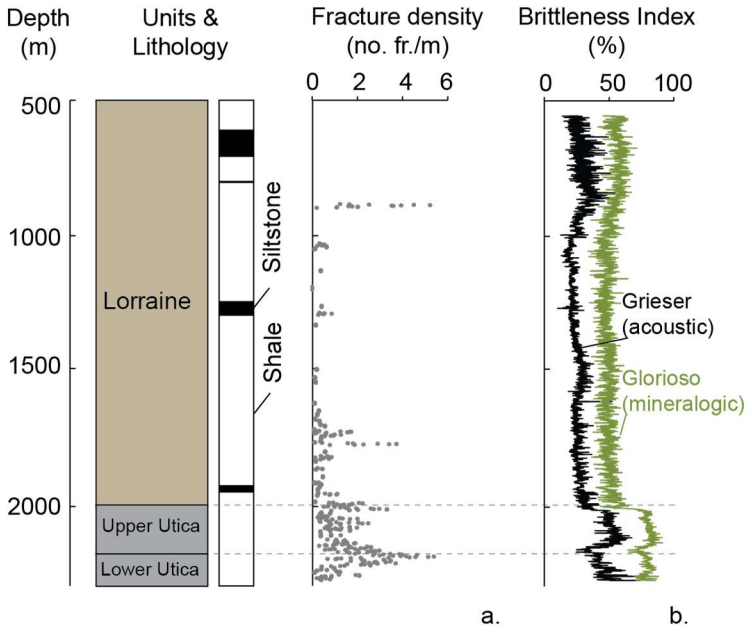

928

929 Fig. 13. Fracture density and rock brittleness at depth: a. example of fracture density variation
930 with depth in the deep vertical well B. Fracture densities were calculated using a 5 m window
931 length every 1 m and the values were corrected for sampling bias; b: mineralogical and acoustic
932 Brittleness Index variations with depth (data from Séjourné (2017)).

933

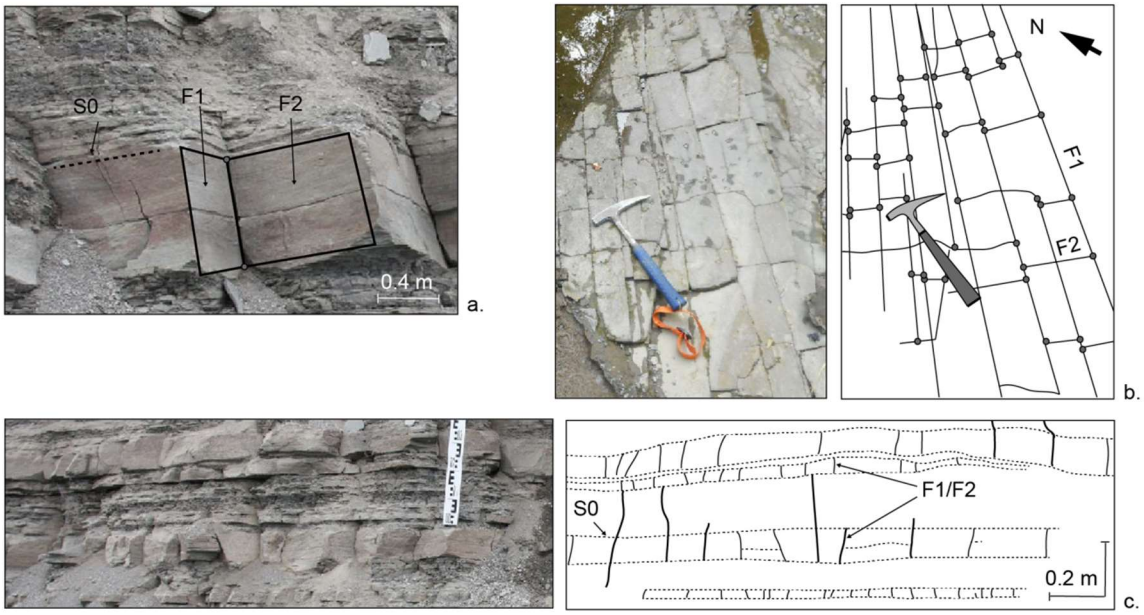

934

935 Fig. 14. Examples of fractures affecting siltstone beds (a and c: site 9; b: top view of the outcrop

936 at site 11). The gray dots highlight the abutting relationships between fracture sets.

937

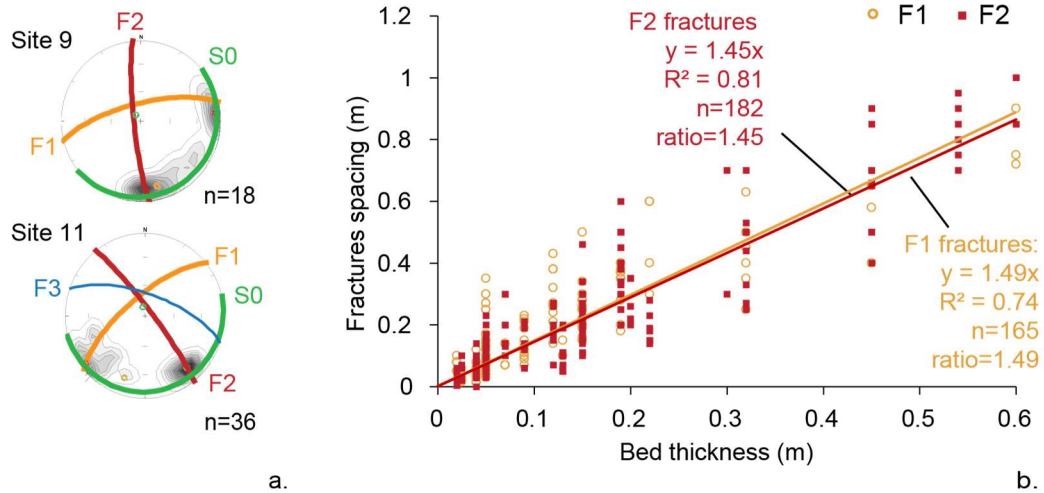

938

939 Fig. 15. Geometrical characteristics of fractures in siltstone units: a. Examples of fracture atti-

940 tudes measured in siltstone outcrops at sites 9 and 11; b. Linear relationship between fracture

spacing and siltstone bed thickness (data from outcrops 1, 6, 13 & 19); the term ratio in the plots corresponds to the fracture spacing to layer thickness ratio; the location of sites is shown in Fig. 1.

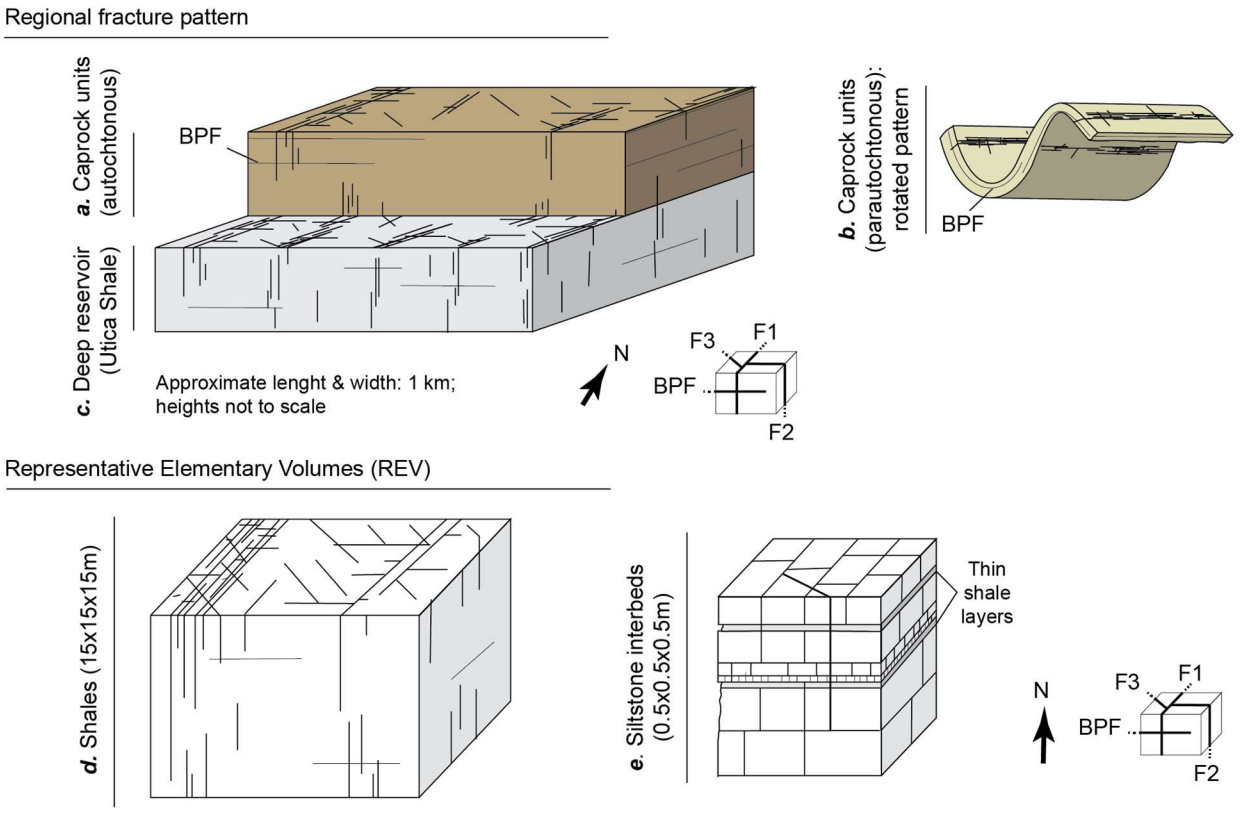

Fig. 16. Conceptual models of the fracture patterns: a. caprock units of the autochthonous domain; b. caprock units of the parautochthonous domain; c. deep shale gas reservoir. In a. and b., the shallow aquifers are not specifically represented because they are affected by the same fracture network than the caprock units. The fracture network is also represented at a smaller scale in REVs: d. shale units; e. siltstone interbeds.